Available online at www.sciencedirect.com

ScienceDirect

Nuclear Physics B 877 (2013) 719–751

NUCLEAR PHYSICS B

www.elsevier.com/locate/nuclphysb

$SO(10)$-inspired solution to the problem of the initial conditions in leptogenesis

Pasquale Di Bari [a,*], Luca Marzola [b]

[a] *School of Physics and Astronomy, University of Southampton, Southampton, SO17 1BJ, UK*
[b] *Institute of Physics, University of Tartu, Tähe 4, EE-51010 Tartu, Estonia*

Received 5 September 2013; accepted 16 October 2013

Available online 5 November 2013

Abstract

We show that, within $SO(10)$-inspired leptogenesis, there exists a solution, with definite constraints on neutrino parameters, able simultaneously to reproduce the observed baryon asymmetry and to satisfy the conditions for the independence of the final asymmetry of the initial conditions (strong thermal leptogenesis). We find that the wash-out of a pre-existing asymmetry as large as $\mathcal{O}(0.1)$ requires: (i) reactor mixing angle $2^\circ \lesssim \theta_{13} \lesssim 20^\circ$, in agreement with the experimental result $\theta_{13} = 8^\circ$–10°; (ii) atmospheric mixing angle $16^\circ \lesssim \theta_{23} \lesssim 41^\circ$, compatible only with current lowest experimentally allowed values; (iii) Dirac phase in the range $-\pi/2 \lesssim \delta \lesssim \pi/5$, with the bulk of the solutions around $\delta \simeq -\pi/5$ and such that $\text{sign}(J_{\text{CP}}) = -\text{sign}(\eta_B)$; (iv) neutrino masses m_i normally ordered; (v) lightest neutrino mass in the range $m_1 \simeq 15$–25 meV, corresponding to $\sum_i m_i \simeq 85$–105 meV; (vi) neutrinoless double beta decay ($0\nu\beta\beta$) effective neutrino mass $m_{ee} \simeq 0.8 m_1$. All together this set of predictive constraints characterises the solution quite distinctively, representing a difficultly forgeable, fully testable, signature. In particular, the predictions $m_{ee} \simeq 0.8 m_1 \simeq 15$ meV can be tested by cosmological observations and (ultimately) by $0\nu\beta\beta$ experiments. We also discuss different interesting aspects of the solution such as theoretical uncertainties, stability under variation of the involved parameters, forms of the orthogonal and RH neutrino mixing matrices.

1. Introduction

Leptogenesis [1,2] is a cosmological application of the see-saw mechanism [3], successfully linking two seemingly independent experimental observations: the matter–antimatter asymmetry of the Universe and the neutrino (masses and mixing) parameters tested in low energy

* Corresponding author.

0550-3213
http://dx.doi.org/10.1016/j.nuclphysb.2013.10.027

neutrino experiments. The matter–antimatter asymmetry can be expressed in terms of the baryon-to-photon number ratio, quite precisely and accurately determined by CMB observations, in particular from Planck (anisotropies plus lensing) data [4]

$$\eta_B^{\rm CMB} = (6.065 \pm 0.090) \times 10^{-10}. \tag{1}$$

On quantitative grounds, the requirement of successful leptogenesis is nicely supported by neutrino oscillation experiments measuring the atmospheric and the solar neutrino mass scales within an optimal (order-of-magnitude) range [5].

If one considers the so-called vanilla scenario, where lepton flavour effects are neglected, a hierarchical RH neutrino spectrum is assumed and the asymmetry is dominantly produced by the lightest RH neutrinos, one obtains an upper bound on the neutrino masses $m_i \lesssim 0.1$ eV [6,7]. As a sufficient (but not necessary) condition that guarantees the final asymmetry to be independent of the initial conditions (strong thermal leptogenesis), a lower bound $m_1 \gtrsim 0.001$ eV on the lightest neutrino mass is also easily obtained. This neutrino mass window [8] is quite interesting since in this way one obtains (at least partially) a testable quantitative link between the matter-antimatter asymmetry and the absolute neutrino mass scale.

However, any attempt to derive further connections with the low energy neutrino parameters encounters serious difficulties, mainly for two reasons: the first is that, within the minimal picture, the right-handed (RH) neutrinos responsible for the generation of the asymmetry are too heavy to give any observational trace, except for the matter–antimatter asymmetry itself; the second is that, by just combining the requirement of successful leptogenesis with low energy neutrino data, there is not a model independent way to over-constrain the see-saw parameter space obtaining testable predictions on future low energy neutrino results. In particular, the final asymmetry is completely independent of the parameters in the leptonic mixing matrix tested by neutrino oscillation experiments.

When lepton flavour effects are taken into account [9], the final asymmetry does depend explicitly on the leptonic mixing matrix. This could raise the hope that leptogenesis can be tested with neutrino oscillations experiments. However, the final asymmetry generally still depends also on the high energy parameters, associated to the properties of the heavy RH neutrinos. It turns out that the observed value of the asymmetry can be attained for an arbitrary choice of the low energy neutrino parameters. As a consequence, inclusion of flavour effects does not lead to new model independent predictions or links with the low energy neutrino parameters. This remains true even within restricted scenarios such as the usual N_1-dominated leptogenesis scenario [10] or the two RH neutrino scenario [11].

Flavour effects have also an impact on the validity of the above mentioned neutrino mass window and in particular of the lower bound $m_1 \gtrsim 10^{-3}$ eV, originating from an intriguing conspiracy between the measured atmospheric and solar neutrino mass scales and the condition of successful strong thermal leptogenesis. This is because, when flavour effects are considered, it is much easier for a pre-existing asymmetry to escape the RH neutrino wash-out [12]. A solution to the requirement of successful strong thermal leptogenesis still exists, but the conditions for its realisation become seemingly quite special. First of all they imply a tauon N_2-dominated scenario, where the final asymmetry is produced by the next-to-lightest RH neutrinos in the two-flavour regime, implying 10^{12} GeV $\gtrsim M_2 \gtrsim 10^9$ GeV, dominantly in the tauon flavour and where the lightest RH neutrino mass $M_1 \ll 10^9$ GeV. In addition, there are a few further conditions on the flavoured decay parameters that apparently make the whole set very difficult to be realised in realistic models. Therefore, the inclusion of flavour effects makes much more difficult to satisfy the strong thermal condition.

On the other hand, there are some phenomenologically significant implications of flavour effects. For example, it is interesting that under some conditions on the RH neutrino masses, the same source of CP violation that could give effects in neutrino oscillations, would also be sufficient to explain the observed matter–antimatter asymmetry within the N_1-dominated scenario [13–15]. After the recent discovery of a non-vanishing θ_{13} in long baseline and reactor experiments [16] and subsequent global analyses [17–19] finding

$$8^\circ < \theta_{13} < 10^\circ \quad (\sim 95\% \text{ C.L.}), \tag{2}$$

this scenario would be viable if $|\sin\delta| \simeq 1$ and $M_1 \gtrsim 10^{11}$ GeV. Though the realisation of successful Dirac phase leptogenesis is not motivated within a precise theoretical framework, this scenario could still emerge as an approximated case within some proposed models such as, for example, minimum flavour violation [20] and two RH neutrino models [13,21]. Therefore, in this respect, it will be rather interesting to determine the value of the Dirac phase during the next years.

Another important consequence of flavour effects is that the N_2-dominated scenario [22] applies for a much wider region of the parameter space. This is because the N_2 produced asymmetry can more easily escape the lightest RH neutrino (N_1) wash-out [23] and reproduce the observed asymmetry [5]. An important application of this effect is that it rescues [24] the so-called $SO(10)$-inspired leptogenesis scenario [25–29]. This scenario corresponds to a very well theoretically motivated set of ($SO(10)$-inspired) conditions that over-constrains the see-saw parameter space. In this way the final asymmetry becomes much more sensitive to the low energy neutrino parameters than in the general case. Within an unflavoured description, the final asymmetry is dominated by the lightest RH neutrino contribution. However, in the light of the current neutrino oscillations data, the RH neutrino mass spectrum turns out to be typically highly hierarchical with the lightest RH neutrino mass $M_1 \ll 10^9$ GeV [26–29], well below the lower bound for successful leptogenesis [30]. This result is quite stable under a precise definition of the $SO(10)$-inspired conditions. It just holds barring very fine tuned choices of the parameters around 'crossing-level' solutions where RH neutrino masses are quasi-degenerate [29], CP asymmetries get resonantly enhanced [31] and successful leptogenesis can be attained [32].

On the other hand, when flavour effects are taken into account, the asymmetry produced by the N_2 decays can reproduce the observed asymmetry. Therefore, $SO(10)$-inspired leptogenesis is rescued by a thorough account of lepton and heavy neutrino flavour effects and it becomes viable [24] if some interesting constraints on the low energy neutrino parameters are satisfied [33]. In particular, a lower bound on the lightest neutrino mass, $m_1 \gtrsim 0.001$ eV, holds. Moreover, inverted ordered neutrino masses are only marginally allowed.[1]

There is, however, also another interesting feature of $SO(10)$-inspired leptogenesis [33]: it is potentially able to satisfy the strong thermal condition, since it indeed naturally realises the above mentioned tauon N_2-dominated scenario.

In this paper we investigate in detail this potential feature of $SO(10)$-inspired models to realise successful strong thermal leptogenesis and we indeed show that there exists a subset of the solutions leading to successful $SO(10)$-inspired leptogenesis that also satisfies the strong thermal condition. We show that this novel solution realising strong thermal condition within $SO(10)$-inspired leptogenesis, implies quite sharp and distinctive constraints on the low energy

[1] Generalisations of the see-saw mechanism within left–right symmetric models with both type I and type II terms [34] or with an inverse see-saw [35] provide alternative solutions.

neutrino parameters, in particular on the neutrino masses. Interestingly, these non-trivially overlap with current experimental constraints and, as we discuss, they can be fully tested by future experiments.

The paper is organised as follows. In Section 2 we introduce the notation and review the status of low energy neutrino experimental results. In Section 3 we briefly review the set-up for $SO(10)$-inspired leptogenesis, verifying the results obtained in [33] and presenting new improved scatter plots that strengthen the conclusions of [33] and reveal some new interesting features. In Section 4 we briefly review and motivate the conditions for successful strong thermal leptogenesis. In Section 5, the central section of the paper, we combine strong thermal and $SO(10)$-inspired conditions and show the existence of a solution implying predictive constraints on neutrino parameters, briefly discussing the prospects to test them in next years. In Section 6 we discuss different aspects of this new solution such as theoretical uncertainties, stability under variation of the involved parameters, corresponding forms of the orthogonal and RH neutrino mixing matrices. Finally, in Section 7, we draw the conclusions.

2. See-saw mechanism and low energy neutrino data

Adding three RH neutrinos to the standard model Lagrangian, one per each generation as predicted by $SO(10)$ models, with Yukawa coupling h and a Majorana mass term M, a neutrino Dirac mass term $m_D = hv$ is generated by the vacuum expectation value v of the Higgs boson, like for the other massive fermions and in particular for the charged leptons with Dirac mass matrix m_ℓ. In this way, in the basis where charged lepton and right-handed neutrino mass matrices are diagonal, their Lagrangian mass terms can be written as ($\alpha = e, \mu, \tau$ and $i = 1, 2, 3$)

$$-\mathcal{L}_M = \overline{\alpha_L} D_{m_\ell} \alpha_R + \overline{\nu_{\alpha L}} m_{D\alpha i} N_{iR} + \frac{1}{2} \overline{N^c_{iR}} D_M N_{iR} + \text{h.c.}, \tag{3}$$

where $D_{m_\ell} \equiv \text{diag}(m_e, m_\mu, m_\tau)$ and $D_M \equiv \text{diag}(M_1, M_2, M_3)$, with $M_1 \leqslant M_2 \leqslant M_3$.

In the see-saw limit, for $M \gg m_D$, the spectrum of neutrino mass eigenstates splits into a very heavy set, $N_i \simeq N_{iR} + N^c_{iR}$, with masses almost coinciding with the Majorana masses M_i, and into a light set $\nu_i \simeq \nu_{iL} + \nu^c_{iL}$, with a symmetric mass matrix m_ν given by the see-saw formula

$$m_\nu = -m_D \frac{1}{D_M} m_D^T. \tag{4}$$

This is diagonalised by a unitary matrix U,

$$U^\dagger m_\nu U^\star = -D_m, \tag{5}$$

corresponding to the leptonic mixing matrix, in a way that we can write

$$D_m = U^\dagger m_D \frac{1}{D_M} m_D^T U^\star. \tag{6}$$

Neutrino oscillation experiments measure two light neutrino mass squared differences, Δm^2_{atm} and Δm^2_{sol}. There are two possibilities: either light neutrino masses are normally ordered (NO), with $m_3^2 - m_2^2 = \Delta m^2_{\text{atm}}$ and $m_2^2 - m_1^2 = \Delta m^2_{\text{sol}}$, or they are inversely ordered (IO), with $m_3^2 - m_2^2 = \Delta m^2_{\text{sol}}$ and $m_2^2 - m_1^2 = \Delta m^2_{\text{atm}}$. For NO (IO) it is found, for example in [19] and similarly in [17,18],[2]

[2] We will neglect throughout the paper the small experimental errors on m_{atm} and on m_{sol} since, with very good approximation, all the constraints that we will discuss are insensitive to them.

$$m_{\rm atm} \equiv \sqrt{m_3^2 - m_1^2} = 0.0505(0.0493)\ \text{eV} \quad \text{and} \quad m_{\rm sol} \equiv \sqrt{\Delta m^2_{\rm sol}} = 0.0087\ \text{eV}. \tag{7}$$

In this way there is just one parameter left to be measured in order to determine the so-called absolute neutrino mass scale fixing the three light neutrino masses. This can be conveniently identified with the lightest neutrino mass m_1. The most stringent upper bound on m_1 is derived from cosmological observations. A conservative upper bound on the sum of the neutrino masses has been recently placed by the Planck Collaboration [4]. Combining Planck and high-ℓ CMB anisotropies, WMAP polarisation and baryon acoustic oscillation data it is found $\sum_i m_i \lesssim 0.23$ eV (95% C.L.). When neutrino oscillation results are combined, this translates into an upper bound on the lightest neutrino mass,

$$m_1 \lesssim 0.07\ \text{eV}, \tag{8}$$

showing how cosmological observations start to corner quasi-degenerate neutrinos.

In the NO case we adopt for the leptonic mixing matrix the PDG parametrisation

$$U^{(\rm NO)} = \begin{pmatrix} c_{12}c_{13} & s_{12}c_{13} & s_{13}e^{-{\rm i}\delta} \\ -s_{12}c_{23} - c_{12}s_{23}s_{13}e^{{\rm i}\delta} & c_{12}c_{23} - s_{12}s_{23}s_{13}e^{{\rm i}\delta} & s_{23}c_{13} \\ s_{12}s_{23} - c_{12}c_{23}s_{13}e^{{\rm i}\delta} & -c_{12}s_{23} - s_{12}c_{23}s_{13}e^{{\rm i}\delta} & c_{23}c_{13} \end{pmatrix} \cdot {\rm diag}\left(e^{i\rho}, 1, e^{i\sigma}\right), \tag{9}$$

where $c_{ij} \equiv \cos\theta_{ij}$ and $s_{ij} \equiv \sin\theta_{ij}$. Because of the adopted light neutrino mass labelling convention, in the IO case the leptonic mixing matrix has to be recast simply with a proper relabelling of the column index, explicitly

$$U^{(\rm IO)} = \begin{pmatrix} s_{13}e^{-{\rm i}\delta} & c_{12}c_{13} & s_{12}c_{13} \\ s_{23}c_{13} & -s_{12}c_{23} - c_{12}s_{23}s_{13}e^{{\rm i}\delta} & c_{12}c_{23} - s_{12}s_{23}s_{13}e^{{\rm i}\delta} \\ c_{23}c_{13} & s_{12}s_{23} - c_{12}c_{23}s_{13}e^{{\rm i}\delta} & -c_{12}s_{23} - s_{12}c_{23}s_{13}e^{{\rm i}\delta} \end{pmatrix} \cdot {\rm diag}\left(e^{i\sigma}, e^{i\rho}, 1\right). \tag{10}$$

As already discussed, the reactor mixing angle is found in the range (2). Current global analyses [19] find for the solar mixing angle the 2σ range $32.6^\circ \lesssim \theta_{12} \lesssim 36.3^\circ$.

The atmospheric mixing angle θ_{23}, is now favoured by MINOS results to be non-maximal [36]. This is also confirmed by global analyses [17–19], though with different statistical significance. In [17] θ_{23} is favoured to be in the first octant, finding for NO the 2σ range $36.3^\circ \lesssim \theta_{23} \lesssim 43.6^\circ$. In [18] θ_{23} is also favoured in the first octant for NO but with a very low statistical significance. In [19] the (almost octant symmetric) 2σ range $38^\circ \lesssim \theta_{23} \lesssim 54.3^\circ$ is found for NO. Certainly more data are needed for a robust determination of the octant. As we will see in Section 5, our solution will give quite a clear prediction on this point.

It will also prove useful to introduce the so-called orthogonal (or Casas–Ibarra) parametrisation [37]. The see-saw formula (4) can be recast as an orthogonality condition for a matrix Ω. Through Ω the neutrino Dirac mass matrix can be expressed as

$$m_D = U\sqrt{D_m}\,\Omega\,\sqrt{D_M}. \tag{11}$$

The Ω matrix contains 6 independent high energy parameters encoding the properties of the 3 RH neutrinos (e.g. the 3 lifetimes and the 3 total CP asymmetries) and it is quite useful not only to express the different relevant quantities for the calculation of the asymmetry, and for this reason we will employ it as an intermediate step for the calculation of the asymmetry, but also to characterise see-saw neutrino models.

3. $SO(10)$-inspired leptogenesis

As we discussed in the introduction, without imposing any condition on the nine high energy parameters, the baryon asymmetry has in general to be calculated taking into account both lepton and heavy neutrino flavour effects and the calculation should proceed through the solution of a set of density matrix equations [39,9,41]. The condition of successful leptogenesis, $\eta_B^{\rm lep} = \eta_B^{\rm CMB}$, places an upper bound on the neutrino masses, $m_1 \lesssim 0.12$ eV [6,40,7], holding in the case of N_1-dominated leptogenesis and in the one-flavour regime, for $M_1 \gtrsim 10^{12}$ GeV. This is the only existing model independent link between leptogenesis and low energy neutrino data.

3.1. General setup

Now let us see how, by imposing $SO(10)$-inspired conditions and barring fine-tuned crossing level solutions [29], a RH neutrino mass pattern implying a N_2-dominated leptogenesis scenario necessarily emerges, where the calculation of the asymmetry reduces to a simple analytical expression and the successful leptogenesis bound implies constraints on all low energy neutrino parameters [33].

The neutrino Dirac mass matrix can be diagonalised by a bi-unitary transformation

$$m_D = V_L^\dagger D_{m_D} U_R, \tag{12}$$

where $D_{m_D} \equiv \mathrm{diag}(m_{D1}, m_{D2}, m_{D3})$. The unitary matrix V_L acts on the left-handed neutrino fields operating the transformation from the weak basis to the Yukawa basis. It is the analogous of the CKM matrix in the quark sector, operating the transformation from the down- to the up-quark mass basis.

Inserting the bi-unitary parameterisation for m_D into the diagonalised see-saw formula (6), one can see that U_R diagonalises the matrix

$$M^{-1} \equiv D_{m_D}^{-1} V_L U D_m U^T V_L^T D_{m_D}^{-1}, \tag{13}$$

explicitly $M^{-1} = U_R D_M^{-1} U_R^T$.[3] This expression shows that the RH neutrino mass spectrum, and the matrix U_R, can be expressed in terms of the low energy neutrino parameters, of the three eigenvalues of m_D and of the six parameters in V_L, explicitly $M_i = M_i(m_j, U; V_L, \alpha_k)$ and $U_R = U_R(m_j, U; V_L, \alpha_k)$, where the three α_k are the ratios of the Dirac mass matrix eigenvalues to the three up-quark masses, explicitly

$$m_{D1} = \alpha_1 m_u, \qquad m_{D2} = \alpha_2 m_c, \qquad m_{D3} = \alpha_3 m_t. \tag{14}$$

Notice that so far we have not yet restricted the see-saw parameters space, we have just simply introduced a sort of hybrid parameterisation where, compared to the orthogonal parameterisation (cf. Eq. (11)), the nine parameters (M_i, Ω) are replaced by (α_k, V_L) or compared to the bi-unitary parameterisation the nine high energy parameters (M_i, U_R) are replaced by (m_j, U), i.e. by the nine testable low energy neutrino parameters in m_ν.

We now define $SO(10)$-inspired models those respecting the following set of three (working) assumptions:

[3] This also implies $D_M = U_R M U_R^T$, showing that U_R operates the transformation of the Majorana mass matrix from the Yukawa basis, where m_D is diagonal, to the basis where the Majorana mass matrix is diagonal.

- The matrix V_L is restricted within the range $I \leqslant V_L \leqslant V_{\rm CKM}$, i.e. the three mixing angles in V_L are not larger than the corresponding three mixing angles in the CKM matrix. This is the most important (i.e. restrictive) condition.
- We assume $\alpha_i = \mathcal{O}(1)$.
- We bar regions in the space of parameters around crossing level solutions, where at least two RH neutrino masses are non-hierarchical, more specifically we impose $M_{i+1} \gtrsim 2M_i$ $(i = 1, 2)$.

The last condition, of a hierarchical RH neutrino spectrum, is not restrictive at all. This is because the conditions to realise crossing level solutions for the RH neutrino mass spectra are very fine tuned [29], especially when the successful leptogenesis bound is imposed. The reason is simple: at the level crossings, the CP asymmetries are resonantly enhanced and span many orders of magnitude. Consequently, the baryon asymmetry is very sensitive to tiny variations of the parameters that have to be highly fine tuned in order for the successful leptogenesis condition, $\eta_B^{\rm lep} = \eta_B^{\rm CMB}$, to be satisfied (as an example of a scenario realising a crossing level solution see [38]).

Under these conditions, and given the current low energy neutrino data, the RH neutrino mass spectrum is hierarchical and of the form [28,24]

$$M_1 : M_2 : M_3 = (\alpha_1 m_u)^2 : (\alpha_2 m_c)^2 : (\alpha_3 m_t)^2. \tag{15}$$

In particular, from the second working assumption and given the current low energy neutrino data, it follows that $M_1 \ll 10^9$ GeV while $M_2 \gg 10^9$ GeV. It also follows that all the heaviest RH neutrino (N_3) CP asymmetries are strongly suppressed. In this way the only contribution able to explain the observed asymmetry is that one from next-to-lightest RH neutrino (N_2) decays. Therefore, the only possibility to satisfy the successful leptogenesis bound is within a N_2-dominated scenario. Assuming a thermal scenario, this necessarily requires that the reheating temperature $T_{\rm RH} \sim M_2$. The baryon asymmetry can then be calculated in a double stage, taking into account first the production and wash-out from the N_2's at $T \sim M_2$ and then the lightest RH neutrino wash-out at $T \sim M_1$.

Let us introduce some standard quantities in leptogenesis. The flavoured decay parameters $K_{i\alpha}$ are defined as

$$K_{i\alpha} \equiv \frac{\Gamma_{i\alpha} + \overline{\Gamma}_{i\alpha}}{H(T = M_i)} = \frac{|m_{D\alpha i}|^2}{M_i m_\star}, \tag{16}$$

where the $\Gamma_{i\alpha}$'s and the $\overline{\Gamma}_{i\alpha}$'s can be identified with the zero temperature limit of the flavoured decay rates into α leptons, $\Gamma(N_i \to \phi^\dagger l_\alpha)$, and antileptons, $\Gamma(N_i \to \phi \bar{l}_\alpha)$ in a three-flavour regime, where lepton quantum states can be treated as an incoherent mixture of the three flavour components. The equilibrium neutrino mass $m_\star$ is defined as

$$m_\star \equiv \frac{16\pi^{5/2}\sqrt{g_*}}{3\sqrt{5}} \frac{v^2}{M_{\rm Pl}} \simeq 1.08 \times 10^{-3}\ {\rm eV}. \tag{17}$$

The total decay parameters are simply given by $K_i = K_{ie} + K_{i\mu} + K_{i\tau}$. In the orthogonal parametrisation the flavoured and total decay parameters can be calculated as

$$K_{i\alpha} = \left| \sum_j \sqrt{\frac{m_j}{m_\star}} U_{\alpha j} \Omega_{ji} \right|^2, \qquad K_i = \sum_i \frac{m_j}{m_\star} |\Omega_{ji}|^2. \tag{18}$$

The efficiency factors at the production, for a vanishing initial N_2 abundance, are given by the sum of a negative and of a positive contribution,

$$\kappa(K_{2\alpha}, K_2) = \kappa^{\rm f}_-(K_2, K_{2\alpha}) + \kappa^{\rm f}_+(K_2, K_{2\alpha}), \tag{19}$$

that are approximated by the following expressions [13]

$$\kappa^{\rm f}_-(K_2, K_{2\alpha}) \simeq -\frac{2}{p^0_{2\alpha}}\, e^{-\frac{3\pi}{8} K_{2\alpha}} \left(e^{\frac{p^0_{2\alpha}}{2}\overline{N}(K_2)} - 1\right) \tag{20}$$

and

$$\kappa^{\rm f}_+(K_2, K_{2\alpha}) \simeq \frac{2}{z_B(K_{2\alpha}) K_{2\alpha}} \left(1 - e^{-\frac{K_{2\alpha} z_B(K_{2\alpha}) \overline{N}(K_2)}{2}}\right), \tag{21}$$

where

$$\overline{N}(K_2) \equiv \frac{N(K_2)}{(1+\sqrt{N(K_2)})^2}, \tag{22}$$

$$z_B(K_{2\alpha}) \simeq 2 + 4 K_{2\alpha}^{0.13} e^{-\frac{2.5}{K_{2\alpha}}} = \mathcal{O}(1\text{–}10) \tag{23}$$

and $p^0_{2\alpha} = K_{2\alpha}/K_2$ is the tree level probability that the lepton quantum state produced by a N_2-decay is measured as an α flavour eigenstate. The flavoured CP asymmetries,

$$\varepsilon_{2\alpha} \equiv -\frac{\Gamma_{2\alpha} - \overline{\Gamma}_{2\alpha}}{\Gamma_2 + \overline{\Gamma}_2}, \tag{24}$$

can be calculated from [31]

$$\varepsilon_{2\alpha} \simeq \bar{\varepsilon}(M_2) \left\{ \mathcal{I}^{\alpha}_{23} \xi\left(M_3^2/M_2^2\right) + \mathcal{J}^{\alpha}_{23} \frac{2}{3(M_3^2/M_2^2 - 1)} \right\}, \tag{25}$$

where we defined [22,5,11]

$$\bar{\varepsilon}(M_2) \equiv \frac{3}{16\pi} \frac{M_2 m_{\rm atm}}{v^2}, \qquad \xi(x) = \frac{2}{3} x \left[(1+x) \ln\left(\frac{1+x}{x}\right) - \frac{2-x}{1-x} \right], \tag{26}$$

$$\mathcal{I}^{\alpha}_{23} \equiv \frac{{\rm Im}[m^{\star}_{D\alpha 2} m_{D\alpha 3} (m^{\dagger}_D m_D)_{23}]}{M_2 M_3 \widetilde{m}_2 m_{\rm atm}} \quad \text{and} \quad \mathcal{J}^{\alpha}_{23} \equiv \frac{{\rm Im}[m^{\star}_{D\alpha 2} m_{D\alpha 3} (m^{\dagger}_D m_D)_{32}]}{M_2 M_3 \widetilde{m}_2 m_{\rm atm}}, \tag{27}$$

with $\widetilde{m}_2 \equiv (m^{\dagger}_D m_D)_{22}/M_2 = K_2 m_{\star}$. The quantities $\mathcal{I}^{\alpha}_{23}$ and $\mathcal{J}^{\alpha}_{23}$ can be expressed in the orthogonal parameterisation as [5,15]

$$\mathcal{I}^{\alpha}_{23} = {\rm Im}\left[\sum_{k,h,l} \frac{m_k \sqrt{m_h m_l}}{\widetilde{m}_2 m_{\rm atm}} \Omega^*_{k2} \Omega_{k3} \Omega^*_{h2} \Omega_{l3} U^*_{\alpha h} U_{\alpha l} \right], \tag{28}$$

$$\mathcal{J}^{\alpha}_{23} = {\rm Im}\left[\sum_{k,h,l} \frac{m_k \sqrt{m_h m_l}}{\widetilde{m}_2 m_{\rm atm}} \Omega^*_{k3} \Omega_{k2} \Omega^*_{h2} \Omega_{l3} U^*_{\alpha h} U_{\alpha l} \right]. \tag{29}$$

We can also conveniently define $\varepsilon_{2\tau^\perp} \equiv \varepsilon_{2e} + \varepsilon_{2\mu}$ and $K_{2\tau^\perp} \equiv K_{2e} + K_{2\mu}$, where $\tau^\perp$ indicates a τ orthogonal flavour component that is a coherent superposition of electron and muon components, in this specific case those ones of the leptons ℓ_2 produced in the N_2 decays. In this way the final asymmetry in the N_2-dominated scenario can be calculated using quite simple expressions [23,5,33].

For $M_2 \ll 10^{12}$ GeV, so that the N_2 production occurs in the two-flavour regime, the final asymmetry can be calculated as

$$N^{\rm f}_{B-L} \simeq \frac{K_{2e}}{K_{2\tau^\perp}} \varepsilon_{2\tau^\perp} \kappa(K_{2\tau^\perp}) e^{-\frac{3\pi}{8} K_{1e}} + \frac{K_{2\mu}}{K_{2\tau^\perp}} \varepsilon_{2\tau^\perp} \kappa(K_{2\tau^\perp}) e^{-\frac{3\pi}{8} K_{1\mu}} + \varepsilon_{2\tau} \kappa(K_{2\tau}) e^{-\frac{3\pi}{8} K_{1\tau}}, \tag{30}$$

where we are calculating abundances in a portion of co-moving volume containing one RH neutrino in ultra-relativistic thermal equilibrium (so that $N^{\rm eq}_{N_i}(T \gg M_i) = 1$). On the other hand, for $M_2 \gg 10^{12}$ GeV the production occurs in the one-flavour regime and in this case one can use

$$N^{\rm f}_{B-L} \simeq \varepsilon_2 \kappa(K_2) \left(\frac{K_{2e}}{K_2} e^{-\frac{3\pi}{8} K_{1e}} + \frac{K_{2\mu}}{K_2} e^{-\frac{3\pi}{8} K_{1\mu}} + \frac{K_{2\tau}}{K_2} e^{-\frac{3\pi}{8} K_{1\tau}} \right). \tag{31}$$

These are the expressions for the final asymmetry that we adopt in our calculation. In the end, however, the case $M_2 \gg 10^{12}$ GeV, will prove to be not particularly significant. Finally, the baryon-to-photon number ratio from leptogenesis can be calculated simply using

$$\eta^{\rm lep}_B = a_{\rm sph} \frac{N^{\rm f}_{B-L}}{N^{\rm rec}_\gamma} \simeq 0.96 \times 10^{-2} N^{\rm f}_{B-L}, \tag{32}$$

accounting for sphaleron conversion and photon dilution. It is important to notice that η_B does not depend on α_1 and α_3 [24]. This reduction of the number of parameters in the final asymmetry is a key point for the see-saw parameter space to be over-constrained by the condition of successful leptogenesis, thus resulting into constraints on the low energy neutrino data that allow the scenario to be testable.

To our knowledge, there are five, potentially relevant, approximations in this calculation of the final asymmetry:

- In the intermediate regime, for $M_2 \sim 10^{12}$ GeV, one should calculate the asymmetry solving the density matrix equation. We approximate the calculation simply using Eq. (30) if $M_2 \leqslant 10^{12}$ GeV and Eq. (31) if $M_2 > 10^{12}$ GeV.
- We are neglecting phantom terms [42,41].
- We are neglecting flavour coupling [42].
- We are neglecting the running of neutrino parameters [43] inserting directly, into the expression for the final asymmetry, the results from low energy neutrino experiments.
- We are neglecting momentum dependence.

We will shortly discuss the potential impact of these approximations in Section 6, concluding that actually they work quite well.

3.2. *Constraints on neutrino parameters from scatter plots*

Let us now present the constraints on neutrino parameters obtained imposing the leptogenesis bound, $\eta^{\rm lep}_B = \eta^{\rm CMB}_B$, $SO(10)$-inspired conditions and assuming vanishing initial asymmetries and N_2-abundance. We have fixed $\alpha_2 = 5$. This can be considered a realistic close-to-maximum value yielding conservative results, considering that $M_2 \propto \alpha_2^2$ and that this translates into $\eta^{\rm lep}_B \propto \alpha_2^2$ (as far as $M_2 \lesssim 10^{12}$ GeV).

The asymmetry $\eta_B^{\rm lep}$ is calculated for differently randomly (and uniformly) generated points in a region of the parameter space obeying the $SO(10)$-inspired condition on the unitary matrix V_L (cf. Eq. (12)). The unitary matrix V_L is parameterised exactly as the leptonic mixing matrix U (cf. Eq. (9)) and, therefore, in terms of three mixing angles $(\theta_{12}^L, \theta_{23}^L, \theta_{12}^L)$ and three phases, $(\delta_L, \rho_L, \sigma_L)$. The three mixing angles are randomly scanned within the ranges $0 \leqslant \theta_{12}^L \leqslant 13^\circ$, $0 \leqslant \theta_{23}^L \leqslant 2.5^\circ$, and $0 \leqslant \theta_{13}^L \leqslant 0.2^\circ$, while the three phases simply vary within $[0, 2\pi]$.

Let us now describe the ranges adopted for the mixing angles. In order to compare our results with those previously obtained in [33], we still adopt the old θ_{13} (2σ) range,

$$0 \leqslant \theta_{13} \leqslant 11.5^\circ, \tag{33}$$

mainly determined by the CHOOZ upper bound [44]. However, in all plots, we also highlight the current experimentally allowed much narrower range (cf. Eq. (2)).

Also for the solar mixing angle we will continue, in the scatter plots, to adopt the same 2σ range as in [33] from [45],

$$31.3^\circ \leqslant \theta_{12} \leqslant 36.3^\circ, \tag{34}$$

just slightly larger than the above mentioned 2σ range from current global analyses.

Finally, for the atmospheric mixing angle we conservatively adopt the range

$$35^\circ < \theta_{23} < 52.5^\circ. \tag{35}$$

Compared to the range used in [33] ($38.5^\circ < \theta_{23} < 52.5^\circ$) [45] this is enlarged at low values taking into account, as previously discussed, that MINOS results [36] and one of the global analyses [17] find now that values well lower than 38.5° are allowed. In particular, the MINOS Collaboration find that values as low as 35° are allowed at about 2σ. The Dirac phase and the two Majorana phases are simply varied within $[0, 2\pi]$. Finally, the atmospheric and solar neutrino mass scales are fixed to their best fit values (cf. Eq. (7)) since the experimental errors are sufficiently small that the final asymmetry is not sensitive to them.

Therefore, the parameter scan is made in a 13-dim parameter space: the 6 parameters in V_L plus the 6 parameters in U plus the lightest neutrino mass m_1. We are clearly particularly interested in determining testable constraints on the 7-dim low energy neutrino parameter space. In Fig. 1 we show, imposing[4] $M_3/M_2 > 10$, the results as projections of the allowed regions on the most significant two low energy neutrino parameter planes for NO. Since we show projections on planes it is sufficient to impose $\eta_B^{\rm lep} > \eta_B^{\rm CMB}$ (in practice we imposed $\eta_B > 5.9 \times 10^{-10}$). Two of the panels also contain plots of the constraints on derived parameters such as the effective $0\nu\beta\beta$ neutrino mass $m_{ee} = |\sum_i m_i U_{ei}^2|$ and on the CP invariant $J_{\rm CP} = c_{12}s_{12}c_{23}s_{23}c_{13}^2 s_{13}\sin\delta$. In the case of m_{ee} the dashed band is excluded by the experimental bound $m_{ee} \lesssim 0.75$ eV (95% C.L.) obtained by the Heidelberg–Moscow and CUORICINO experiments (recently tightened by GERDA [46]). The allowed found solutions are indicated with yellow points.[5]

We do not show results for IO since in Section 5 we will point out that IO is incompatible with the strong thermal condition, our main focus in this paper.

Notice that the ranges for the mixing angles shown in the plots are exactly those adopted in the scatter plots (cf. Eqs. (33), (34) and (35)). We find a perfect agreement with the results of [33]

[4] We consider separately the results for $10 \gtrsim M_3/M_2 \gtrsim 2$ and discuss them in Section 6.

[5] The red, green and blue points satisfy, in addition to the successful leptogenesis condition, also the strong thermal condition, as we will discuss in the next sections.

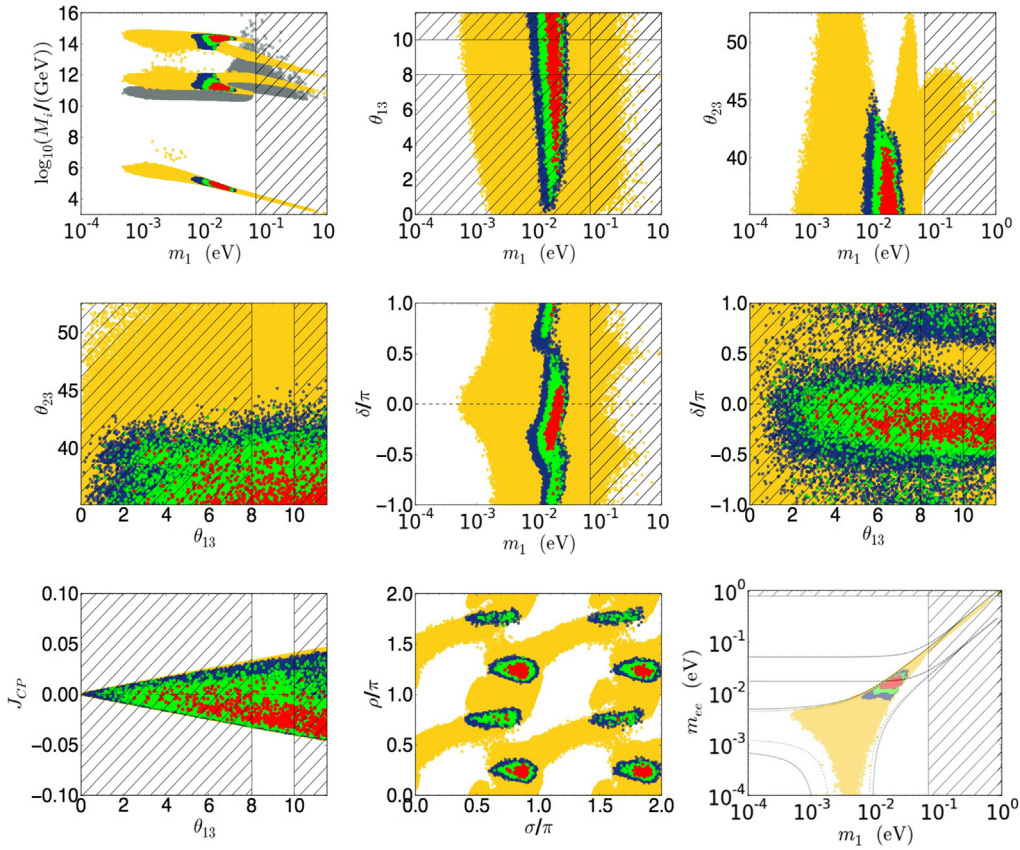

Fig. 1. Scatter plots in the parameter space projected on different planes for NO and $\alpha_2 = 5$. The mixing angles vary within the experimental 2σ ranges (cf. Eqs. (33), (34) and (35)). The dashed regions indicate either the values of m_1 excluded by the CMB upper bound (cf. Eq. (8)), or the values of m_{ee} excluded by $0\nu\beta\beta$ experiments, or the values of θ_{13} excluded by current determination (cf. Eq. (2)). All points satisfy the (2σ) successful leptogenesis bound $\eta_B > \eta_B^{\rm CMB} > 5.9 \times 10^{-10}$. They are obtained imposing both $SO(10)$-inspired and strong thermal conditions for different values of the pre-existing asymmetry. The yellow points correspond to an initial vanishing asymmetry (the strong thermal condition is ineffective). The blue, green and red points are obtained respectively for an initial value of the pre-existing asymmetry $N_{B-L}^{\rm p,i} = 10^{-3}, 10^{-2}, 10^{-1}$. In the bottom right panel the dashed (solid) black lines indicate the general (no leptogenesis) allowed bands, both for NO and IO, in the plane m_{ee} vs. m_1 for θ_{13} in the range (2) (Eq. (33)). (For interpretation of the references to colour in this figure, the reader is referred to the web version of this article.)

(another reason not to show again the results for IO). However, due to an improved computing procedure, we could generate hundred times higher number of points. In this way the borders of the allowed regions are very sharply determined, as it can be noticed from the figure. We fully confirm and strengthen all results found in [33] (we recall that all constraints are obtained for $\alpha_2 = 5$). Let us highlight some of the main features of the found solutions.

3.2.1. Existence of three types of solutions

We confirm that there are only three types of solutions leading to successful $SO(10)$-inspired leptogenesis [24,33]. We will refer to them as τ_A, τ_B and μ-type solutions: the τ_A and τ_B types being characterised by $K_{1\tau} \lesssim 1$, implying a tauon-flavour dominant contribution to the final

asymmetry, while the μ-type being characterised by $K_{1\mu} \lesssim 1$ and, therefore, muon dominated. These three types result respectively into three sets of (partly overlapping) allowed regions, that are now, in our new analysis, quite clearly distinguishable in two of the plots in Fig. 1: in the upper left panel showing the constraints in the plane m_1–M_i and in the upper-right panel showing the constraints in the m_1–θ_{23} plane. In this case it should be noticed how for values $\theta_{23} \gtrsim 45^\circ$ the three types correspond to well distinguished (non-overlapping) allowed regions.

In Fig. 2 we plot, versus m_1, different relevant quantities associated to the three specific sets of parameters specified in the figure caption and realising the three different types: the left panels refer to a τ_A-type solution, the central panels to a τ_B-type solution and the right panels to a μ-type solution. In the bottom panels we plot the contributions to the final asymmetry η_B from the three different flavours and it can be seen how indeed the τ_A and the τ_B-type solutions are tauon-dominated while the μ-type solution is muon dominated. It can be also noticed how the τ_A-type is characterised by $K_{2\tau} \gg 1$ and $K_{1e} \lesssim 1$ for $m_1 \lesssim 10$ meV, while $K_{1e} \gg 1$ for $m_1 \gtrsim 10$ meV. On the other hand, the τ_B-type is characterised by $K_{1e} \gg 1$ for any value of m_1 while $1 \gtrsim K_{2\tau} \gtrsim 20$. These features will be relevant when we will impose the strong thermal condition in order to understand what kind of subset of the solutions satisfy also this additional important property. Let us now discuss the main features of the constraints on the low energy neutrino parameters in the light of these new results resulting from a much higher amount of solutions (about two orders of magnitude) compared to the previous ones obtained in [33].

3.2.2. Lower bound on m_1

First of all we confirm the existence of a lower bound $m_1 \gtrsim 5 \times 10^{-4}$ eV. This can be considered quite a conservative and robust lower bound from $SO(10)$-inspired leptogenesis. The origin of this lower bound is due to the fact that for $m_1 \ll 10^{-3}$ eV one has $M_3 \gg 10^{15}$ GeV and consequently all the N_2 CP asymmetries get suppressed [24,33]. A new feature, that is interesting to notice in the light of the θ_{13} measurement, opening prospects for a measurement of the Dirac phase δ, is that the lower bound on m_1 depends on δ and in particular the lowest value, $m_1 \simeq 5 \times 10^{-4}$ eV, is saturated for $\delta \simeq 0$, while for $|\delta| \gtrsim \pi/2$, as very weakly supported by current global analyses, one has $m_1 \gtrsim 10^{-3}$ eV. Therefore, in these models, a determination of δ shows an interesting interplay with absolute neutrino mass scale experiments.

3.2.3. Upper bound on θ_{23} for quasi-degenerate neutrinos

Another interesting constraint of this scenario, found in [33] and confirmed by our analysis, is the existence of an upper bound on θ_{23} for sufficiently large values of m_1, the μ type region. Our new results confirm this constraint as well. This is now determined quite accurately and precisely: $\theta_{23} \lesssim 48^\circ$ for $m_1 \gtrsim 60$ meV. It should be noticed that the new upper bound from Planck data (cf. Eq. (8)) now basically almost completely rules out this μ type region at high m_1 values.

3.2.4. Majorana phases

As it can be seen in the lower central panel of Fig. 1, the Majorana phases cannot have arbitrary values but there are some quite large excluded regions. Our results for $\alpha_2 = 5$ are fully compatible with the results found in [33]. In [33] results were found for $\alpha_2 = 4, 5$ and showed that the Majorana phases tend to cluster dominantly around disconnected regions for values $\rho \simeq (n + 1/2)\pi$ and $\sigma \simeq n\pi$ and sub-dominantly around regions for $\rho, \sigma \simeq n\pi$. Now, since we have found a much greater amount of solutions, the regions are sharply determined and for $\alpha_2 = 5$ the allowed regions are connected. However, the bulk of points still falls around the same values

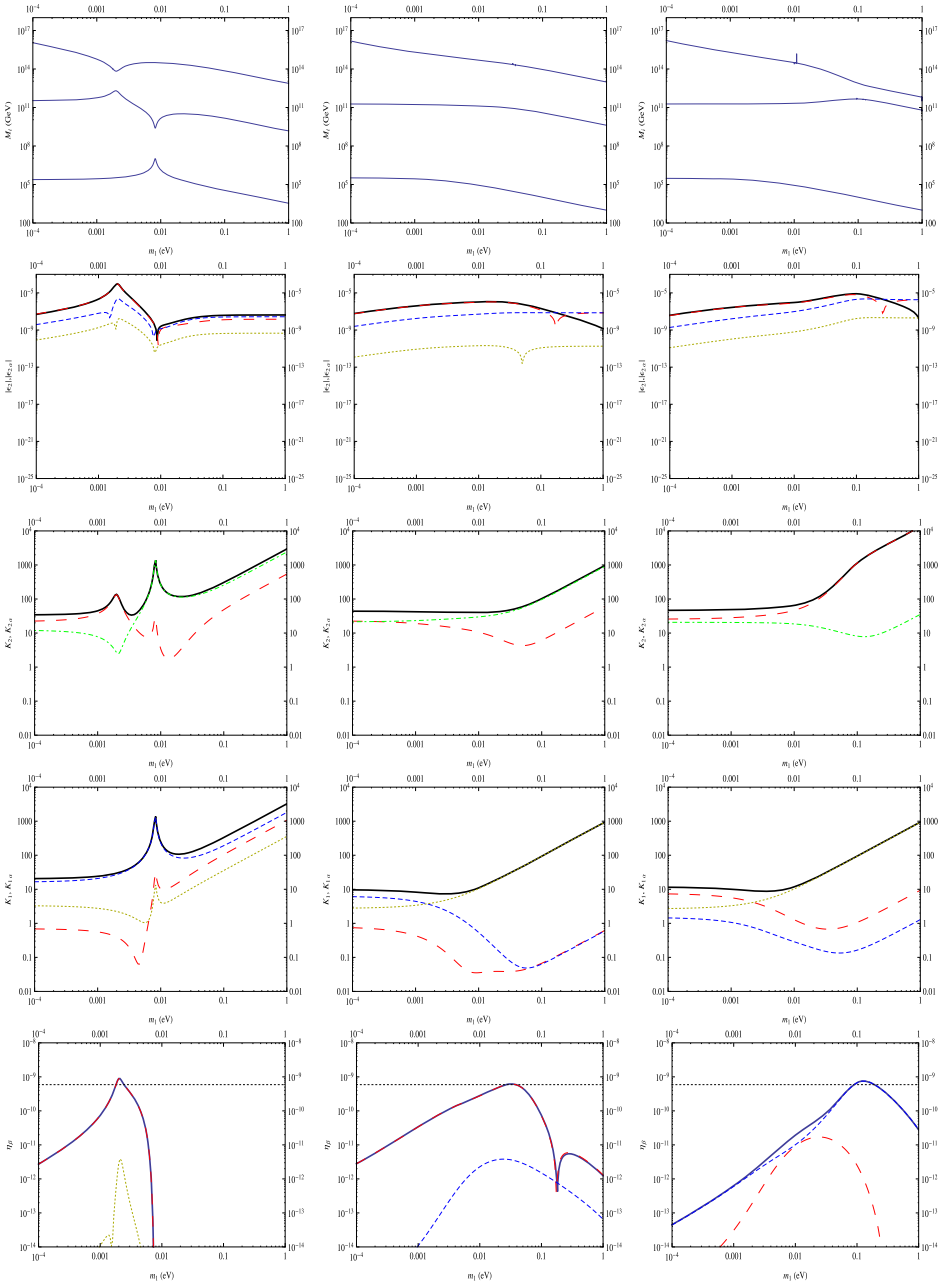

Fig. 2. Plots of the relevant quantities for the three following sets of parameters: $\theta_{13} = (7.9^\circ, 2.8^\circ, 1.4^\circ)$, $\theta_{12} = (34^\circ, 34.6^\circ, 36^\circ)$, $\theta_{23} = (50^\circ, 48^\circ, 46^\circ)$, $\delta = (-0.29, -0.28, 0.56)$, $\rho = (1.4, 6.24, 3.17)$, $\sigma = (3.14, 6.02, 4.75)$, $\theta_{13}^L = (0.14^\circ, 0.14^\circ, 0.037^\circ)$, $\theta_{12}^L = (6.0^\circ, 0.41^\circ, 5.8^\circ)$, $\theta_{23}^L = (2.1^\circ, 2.1^\circ, 1.24^\circ)$, $\rho_L = (1.15, 0.68, 5.1)$, $\sigma_L = (3.7, 3.24, 2.4)$, corresponding respectively to τ_A, τ_B and μ-type solutions. The long-dashed red lines correspond to $\alpha = \tau$, the dashed blue lines to $\alpha = \mu$ and the short-dashed dark yellow lines to $\alpha = e$. For all three cases $(\alpha_1, \alpha_2, \alpha_3) = (1, 5, 1)$, though notice that, except for the three RH neutrino masses, all quantities are independent of α_1 and α_3. (For interpretation of the references to colour in this figure, the reader is referred to the web version of this article.)

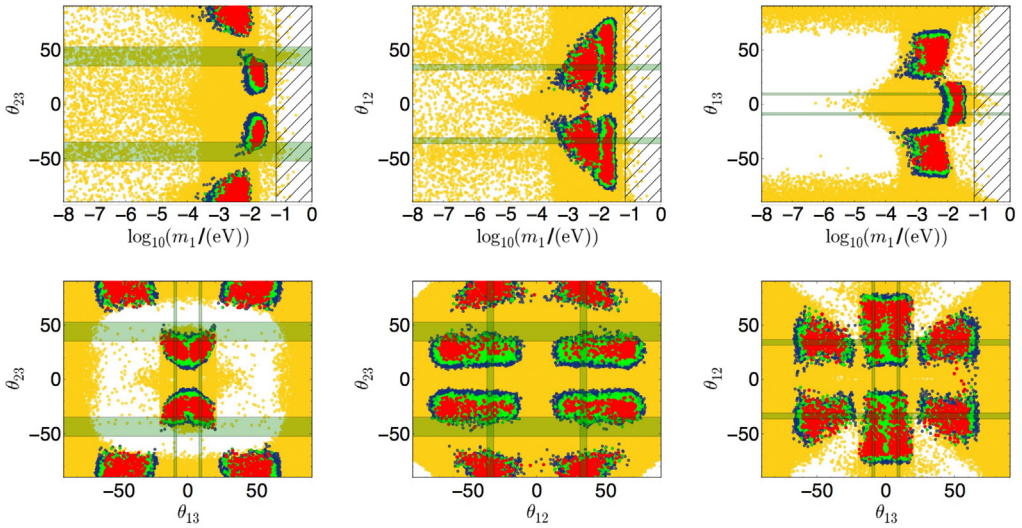

Fig. 3. Scatter plots as in Fig. 1 but without imposing the experimental information on mixing angles from neutrino oscillation experiments. Mixing angles are shown in the range $[-90°, 90°]$ since the addition of a Majorana mass term with three RH neutrinos introduces a sign sensitivity (differently from neutrino oscillations probabilities). In our case since the asymmetry is generated by just one RH neutrino there is no sign sensitivity and the regions at negative values just mirror those at positive values. (For interpretation of the references to colour in this figure, the reader is referred to the web version of this article.)

found in [33]. The differences are then just simply to be ascribed to the much higher number of determined points.

3.2.5. *Dirac phase and J_{CP}*

The results for the Dirac phase and for the Jarlskog invariant,

$$J_{\mathrm{CP}} = \mathrm{Im}\left[U_{\mu 3} U_{e2} U^{\star}_{\mu 2} U^{\star}_{e3}\right] = c_{12} s_{12} c_{23} c^2_{13} s_{13} \sin\delta, \tag{36}$$

do not show any constraint and, in particular, no preference for the sign. Compared to the results found in [33] we have just found a trivial bug in the plot of J_{CP} vs. θ_{13} shown in [33] where θ_{13} was displayed for $\theta_{13} \lesssim 11.5°$ in radians instead of degrees as indicated.

3.3. *Are the low energy neutrino data pointing in the right direction?*

A particularly interesting test was performed in [33]. The allowed regions for the low energy neutrino parameters were also determined without imposing any restriction from low energy neutrino experiments. In this way one can test how predictive the scenario is and whether the agreement with current experimental data is particularly significant. We have repeated this test and the results are shown in Fig. 3. Also in this case we confirm the results of [33]. The huge amount of points now clearly determines the existence of excluded regions. The fact that the experimental results (the green bands) fall in the allowed regions represents a positive test of the model. In particular, it is quite interesting to notice (see yellow points in the left bottom panel) that the measured value of θ_{13} implies that the atmospheric mixing angle range $50° \lesssim \theta_{23} \lesssim 70°$ is excluded or that for the measured values of θ_{23} the range of values $20° \lesssim \theta_{13} \lesssim 60°$ is excluded.

However, the allowed (yellow) regions cover a large portion of the parameter space and, therefore, the test is not particularly statistically significant. In other words, neutrino data could have already ruled out $SO(10)$-inspired leptogenesis, but the probability that they just by chance fall within the $SO(10)$ allowed regions is too high to draw any statistically significant conclusion. Indeed, if one looks at the mixing angles, one could say that there was roughly just a 50% probability that the data could exclude $SO(10)$-inspired leptogenesis. As we will see, the situation drastically changes when the strong thermal leptogenesis condition is further imposed.

4. The strong thermal leptogenesis condition

We have so far assumed that the observed asymmetry is entirely generated by leptogenesis. However, there are other possible external mechanisms, such as gravitational baryogenesis [47] and Affleck–Dine baryogenesis [48], able to generate an asymmetry prior the onset of leptogenesis. In particular, so-called grand unified baryogenesis models [49], are particularly relevant within our context, since this would be quite a natural and extensively studied possibility arising just within grand unified $SO(10)$ models inspiring the scenario we are discussing. Moreover, they are particularly well motivated considering the large initial temperatures required by minimal thermal leptogenesis (though a non-thermal production would be also plausible).

These potential sources would compete with leptogenesis and in general, at the large initial reheat temperature required by (minimal) thermal leptogenesis and in particular by $SO(10)$-inspired leptogenesis, $T_{\rm RH} \gtrsim 10^{11}$ GeV, they would typically produce a pre-existing asymmetry well above the observed one, up to values $\mathcal{O}(0.1)$.

Clearly one possibility would be to assume that at the end of the inflationary stage any asymmetry was completely erased and that no mechanism had efficiently produced a pre-existing asymmetry prior the onset of leptogenesis. However, it would be quite attractive, and the constraints on low energy neutrino parameters much more significant, if the same processes involving RH neutrinos could wash-out any pre-existing asymmetry and at the same time produce a final value of the asymmetry independent of the initial RH neutrino abundances (strong thermal leptogenesis condition). This would be an analogous situation compared to what happens in Standard Big Bang Nucleosynthesis.

Let us translate this request in quantitative terms. In the presence of an initial pre-existing asymmetry, the predicted value of the final $B-L$ asymmetry would be in general the sum of the residual value of the pre-existing asymmetry, $N^{\rm p,f}_{B-L}$, plus the genuine leptogenesis contribution from RH neutrino decays, $N^{\rm lep,f}_{B-L}$, or, in terms of the baryon-to-photon number ratio at the present time,

$$\eta_B = \eta^{\rm p}_B + \eta^{\rm lep}_B, \tag{37}$$

where $\eta^{\rm p}_B$ and $\eta^{\rm lep}_B$ are simply given by Eq. (32) by replacing $N^{\rm f}_{B-L}$ respectively with $N^{\rm p,f}_{B-L}$ and $N^{\rm lep,f}_{B-L}$. The condition of *successful strong thermal leptogenesis* can then be expressed as [12]

$$\left|\eta^{\rm p}_B\right| \ll \eta^{\rm lep}_B \simeq \eta^{\rm CMB}_B. \tag{38}$$

Within the simple vanilla leptogenesis scenario, where the asymmetry is N_1-dominated and flavour effects are neglected, the relic value of the pre-existing $B-L$ asymmetry is simply given by [1,8]

$$N^{\rm p,f}_{B-L} = N^{\rm p,i}_{B-L} e^{-\frac{3\pi}{8}K_1}. \tag{39}$$

Considering the relation (32) between $N^{\rm f}_{B-L}$ and η_B, it is, therefore, simply sufficient to impose $K_1 \gtrsim 15 + \ln N^{\rm p,i}_{B-L}$ to enforce the strong thermal leptogenesis condition.

When flavour effects are taken into account, and considering hierarchical RH neutrino mass patterns, as we are considering within $SO(10)$-inspired models, strong thermal leptogenesis can be realised only within a tauon-dominated N_2-dominated scenario where the dominant contribution to the asymmetry is in the tauon flavour [12]. This is because, if $M_2 \lesssim 10^{12}$ GeV, the tauon components of the lepton and antilepton quantum states can be measured before the asymmetry is produced by the N_2-decays. In this way the τ component of the pre-existing asymmetry can be washed-out by the N_2 inverse processes if $K_{2\tau} \gg 1$, and at the same time a new tauon component can be afterwards generated by the out-of-equilibrium N_2 decays. On the other hand, for a generic model, the e and the μ components can be fully washed-out only in the three-flavour regime by the N_1 wash-out, i.e. after the N_2 leptogenesis, so that they cannot be afterwards regenerated contributing to $\eta^{\rm lep}_B$.

As we have seen, the tauon dominance condition is naturally satisfied by two of the three types of solutions found in $SO(10)$-inspired leptogenesis.[6] This, therefore, represents quite a well motivated theoretical framework that is a potential candidate to realise successful strong thermal leptogenesis.

The request of the successful strong thermal condition, however, goes beyond the tauon dominance since it also requires quite restrictive additional conditions onto the flavoured decay parameters. These additional conditions can be fully understood calculating explicitly the residual value of the pre-existing asymmetry.

First of all, we can safely assume that the heaviest RH neutrinos are too heavy to be thermally produced and, therefore, they do not contribute to the wash-out of the pre-existing asymmetry. This is clearly a conservative assumption since the presence of the heaviest RH neutrino can only introduce an additional wash-out stage of the pre-existing asymmetry. However, it should be taken into account that, since $M_3 \gg 10^{12}$ GeV the N_3 wash-out acts on a ℓ_3 flavour direction and, therefore, it is in general not really helpful in washing out the pre-existing asymmetry, not even along the τ direction [12]. For this reason an inclusion of such a wash-out would not have in any case any impact on the constraints we will find.

Therefore, if a pre-existing asymmetry is generated at $T \geqslant T^{\rm ext}_B$ by some external mechanism, at a later stage, for temperatures $T^{\rm ext}_B \gg T \gg M_2$, this simply remains constant,

$$N^{\rm p}_{B-L}(T \gg M_2) = N^{\rm p,i}_{B-L}. \tag{40}$$

For temperatures 10^{12} GeV $\gg T \gg M_2$, because of the fast tauon lepton interactions, the quantum lepton states become an incoherent admixture of a tauon component and of a τ orthogonal component $\tau^{\perp}$. The initial pre-existing asymmetry can then be regarded as the sum of two components

$$N^{\rm p}_{B-L} = N^{\rm p,i}_{\Delta_\tau} + N^{\rm p,i}_{\Delta_{\tau^\perp}} \quad \left(10^{12}\ {\rm GeV} \gg T \gg M_2\right), \tag{41}$$

related to the total pre-existing asymmetry simply by

[6] Notice that this does not happen by chance. Since one assumes the hierarchy of neutrino Yukawa couplings like for up-quarks (and similarly for the charge leptons) Yukawa couplings, the fact that the tauon flavour component is the first to become incoherent at $T \lesssim 10^{12}$ GeV, the reason why one needs a tauon N_2-dominated scenario to satisfy the strong thermal condition, reflects typically into a dominant tauon CP asymmetry ($\propto \alpha_3^2$) and, therefore, naturally into a tauon N_2-dominated scenario within $SO(10)$-inspired models.

$$N^{\rm p,i}_{\Delta_\tau} = p^0_{\rm p\tau} N^{\rm p,i}_{B-L}, \qquad N^{\rm p,i}_{\Delta_{\tau^\perp}} = \big(1-p^0_{\rm p\tau}\big) N^{\rm p,i}_{B-L}, \tag{42}$$

where $p^0_{p\tau}$ is the tree-level probability of pre-existing leptons to be in the tauon flavour. In principle, there could be differences in the pre-existing lepton–antilepton flavour compositions and these would translate into additional opposite contributions to the flavoured asymmetries, the so-called phantom terms, that, however we can simply neglect in order to simplify the notation. We will point out in the end that all results are valid also in the presence of these additional terms.

For temperatures $T \sim M_2$ the N_2 processes at the same time will generate a contribution to $N^{\rm lep}_{B-L}$ and wash-out the pre-existing flavoured asymmetries. However, these processes cannot wash-out the component $\tau^\perp_{2^\perp}$ of the pre-existing asymmetry, i.e. the projection on the e–μ plane orthogonal to the heavy neutrino lepton flavour ℓ_2. At the end of this stage, at $T \simeq T_{B2} \simeq M_2/z_{B2}$, the residual values of the pre-existing asymmetries will be then given by three components,

$$\begin{aligned}
&N^{\rm p}_{\Delta_\tau}(T_{B2}) = p^0_{\rm p\tau} e^{-\frac{3\pi}{8}K_{2\tau}} N^{\rm p,i}_{B-L},\\
&N^{\rm p}_{\Delta_{\tau^\perp_2}}(T_{B2}) = \big(1-p^0_{\rm p\tau}\big) p^0_{p\tau^\perp_2} e^{-\frac{3\pi}{8}(K_{2e}+K_{2\mu})} N^{\rm p,i}_{B-L},\\
&N^{\rm p}_{\Delta_{\tau^\perp_{2^\perp}}}(T_{B2}) = \big(1-p^0_{\rm p\tau}\big)\big(1-p^0_{p\tau^\perp_2}\big) N^{\rm p,i}_{B-L}.
\end{aligned} \tag{43}$$

At temperatures $T \sim 10^9$ GeV, also muon lepton interactions become effective, breaking the residual coherence of the e–μ lepton components in way that in the range $10^9\ {\rm GeV} \gg T \gg M_1$ the total asymmetry can be regarded as the sum of three charged lepton flavour components

$$N^{\rm p}_{B-L}\big(10^9\ {\rm GeV} \gg T \gg M_1\big) = \sum_{\alpha=e,\mu,\tau} N^{\rm p}_{\Delta_\alpha}(T_{B2}), \tag{44}$$

where

$$\begin{aligned}
&N^{\rm p}_{\Delta_\tau}\big(10^9\ {\rm GeV} \gg T \gg M_1\big) = p^0_{\rm p\tau} e^{-\frac{3\pi}{8}K_{2\tau}} N^{\rm p,i}_{B-L},\\
&N^{\rm p}_{\Delta_\mu}\big(10^9\ {\rm GeV} \gg T \gg M_1\big)\\
&\quad = \big(1-p^0_{\rm p\tau}\big)\big[p^0_{\mu\tau^\perp_2} p^0_{p\tau^\perp_2} e^{-\frac{3\pi}{8}(K_{2e}+K_{2\mu})} + \big(1-p^0_{\mu\tau^\perp_2}\big)\big(1-p^0_{p\tau^\perp_2}\big)\big] N^{\rm p,i}_{B-L},\\
&N^{\rm p}_{\Delta_e}\big(10^9\ {\rm GeV} \gg T \gg M_1\big)\\
&\quad = \big(1-p^0_{\rm p\tau}\big)\big[p^0_{e\tau^\perp_2} p^0_{p\tau^\perp_2} e^{-\frac{3\pi}{8}(K_{2e}+K_{2\mu})} + \big(1-p^0_{e\tau^\perp_2}\big)\big(1-p^0_{p\tau^\perp_2}\big)\big] N^{\rm p,i}_{B-L}
\end{aligned} \tag{45}$$

and where the probabilities $p^0_{\alpha\tau^\perp_2}$ are unambiguously expressed in terms of the decay parameters,

$$p^0_{e\tau^\perp_2} = \frac{p^0_{2e}}{p^0_{2e}+p^0_{2\mu}} = \frac{K_{2e}}{K_{2e}+K_{2\mu}}, \tag{46}$$

analogously for $p^0_{\mu\tau^\perp_2}$. These expressions now clearly show that the tauon component is the only component of the pre-existing asymmetry that can be completely washed-out by the N_2 wash-out processes.

Finally, at temperatures $T \sim M_1$, the lightest RH neutrino wash-out processes act on the flavoured asymmetries in a way that the relic values of the pre-existing asymmetries flavoured components are given by

$$
\begin{aligned}
N^{\mathrm{p,f}}_{\Delta_\tau} &= p^0_{\mathrm{p}\tau} e^{-\frac{3\pi}{8}(K_{1\tau}+K_{2\tau})} N^{\mathrm{p,i}}_{B-L},\\
N^{\mathrm{p,f}}_{\Delta_\mu} &= \big(1-p^0_{\mathrm{p}\tau}\big) e^{-\frac{3\pi}{8}K_{1\mu}}\big[p^0_{\mu\tau_2^\perp} p^0_{p\tau_2^\perp} e^{-\frac{3\pi}{8}(K_{2e}+K_{2\mu})} + \big(1-p^0_{\mu\tau_2^\perp}\big)\big(1-p^0_{p\tau_2^\perp}\big)\big] N^{\mathrm{p,i}}_{B-L},\\
N^{\mathrm{p,f}}_{\Delta_e} &= \big(1-p^0_{\mathrm{p}\tau}\big) e^{-\frac{3\pi}{8}K_{1e}}\big[p^0_{e\tau_2^\perp} p^0_{p\tau_2^\perp} e^{-\frac{3\pi}{8}(K_{2e}+K_{2\mu})} + \big(1-p^0_{e\tau_2^\perp}\big)\big(1-p^0_{p\tau_2^\perp}\big)\big] N^{\mathrm{p,i}}_{B-L}.
\end{aligned}
\tag{47}
$$

The most reasonable assumption for the flavour composition of the pre-existing asymmetry is that $p^0_{p\alpha} \simeq 1/3$, equivalent to assume that the source is flavour blind. In any case, as we will comment, the results are basically insensitive to specific choices, unless one select special values corresponding, for example, to a pre-existing asymmetry entirely in one specific charged lepton flavour. In this special case it would be much easier to wash-out the pre-existing asymmetry but on the other hand this would be analogous to assuming a vanishing initial asymmetry, while we are interested in finding the general conditions for the independence of the initial conditions. We have, therefore, set $p^0_{p\alpha} = \mathcal{O}(0.1)$.

The expression (47) now explicitly shows that, in order for successful strong thermal leptogenesis to be realised, the final asymmetry has to be necessarily tauon dominated. This is because only in the tauon flavour the wash-out of the pre-existing asymmetry by the N_2 inverse processes at $T \sim M_2$ for $K_{2\tau} \gg 1$ does not prevent that a genuine leptogenesis contribution is afterwards generated by the same N_2 decays at $T \simeq T_{B2} \ll M_2$, surviving until the present time for $K_{1\tau} \lesssim 1$. On the other hand, the electron and muon components of the pre-existing asymmetries can be only fully washed-out by the N_1 wash-out processes at $T \sim M_1$ for $K_{1e}, K_{1\mu} \gg 1$.[7] However, this unavoidably implies that together also the electron and muon leptogenesis contribution from N_2 decays is washed-out, while the N_1 decays are ineffective in generating a sizeable asymmetry. In this way the final asymmetry has necessarily to be tauon dominated.

Therefore, the full set of conditions on the flavoured decay parameters can be summarised as [12]

$$
K_{1e} \gg 1, \qquad K_{1\mu} \gg 1, \qquad K_{2\tau} \gg 1, \qquad K_{1\tau} \lesssim 1,
\tag{48}
$$

with the precise values depending on the precise assumed values of $N^{\mathrm{p,i}}_{B-L}$.

The same set of conditions is sufficient also if one relaxes the assumption that the pre-existing leptons and antileptons quantum states are not CP conjugated of each other. In this case the only difference is that in the three-flavour regime one would have additional contributions to $N^{\mathrm{p,f}}_{\Delta\alpha}$ with $\alpha = e, \mu$ in Eq. (47) inside the squared brackets, that are anyway washed-out when $K_{1e}, K_{1\mu} \gg 1$.[8]

In the next section we will see how this seemingly quite restrictive set of conditions (cf. Eq. (48)) can be indeed realised within $SO(10)$ inspired leptogenesis, translating into quite an interesting set of constraints on the low energy neutrino parameters, sharp enough to be regarded as a quite distinctive signature of the scenario.

[7] There is a caveat: this conclusion does not hold for fine tuned models where the ℓ_2 tauon orthogonal component is purely electronic or muonic with huge precision such that $1 - p^0_{\alpha\tau_2^\perp} \simeq 0$ ($\alpha = e$ or μ). These models would effectively correspond to two-flavour models. In any case this special situation is not realised in $SO(10)$-inspired models under consideration.

[8] Notice that in the presence of phantom terms in the pre-existing asymmetry the caveat pointed out in footnote 4 does not apply.

Before concluding this section, we would just like to make a brief comment on the possible existence of a source of baryogenesis posterior to leptogenesis. In this case there is clearly no condition that can be imposed for its wash-out. Simply there should be no experimental evidence for new physics supporting an alternative mechanism of baryogenesis. While a pre-existing asymmetry would be difficultly testable, a posterior production is more likely to be testable. In this case baryogenesis would occur in a post-inflationary stage during the standard radiation regime. Basically the only realistic known source to be competitive with leptogenesis would come from some realisation of electroweak baryogenesis typically requiring some extension of the Standard Model testable at colliders. If some signal of new physics will be found, it would then become important to constraint such a possibility for an alternative production of the asymmetry after leptogenesis. Since the LHC has not provided evidence for new physics so far, we do not have to worry of any additional condition to be imposed.

5. Strong thermal $SO(10)$-inspired solution

5.1. Results on neutrino parameters

We have imposed the strong thermal condition Eq. (38) on the solutions with $M_2 < 10^{12}$ GeV found within the $SO(10)$-inspired scenario discussed in Section 3[9] finding that this is indeed satisfied by a subset of them. This has been done for three different values of the initial pre-existing $B - L$ asymmetry $N^{\rm p,i}_{B-L}$.

The results can be read off from the same panels of Fig. 1. The solutions are indicated with blue, green and red points respectively for $N^{\rm p,i}_{B-L} = 10^{-3}, 10^{-2}$ and 10^{-1}. One can see that in the different neutrino parameter planes, the regions satisfying the strong thermal condition are clearly a subset of the allowed regions within $SO(10)$-inspired leptogenesis (the yellow points). In some cases they introduce such strong and definite constraints on the low energy neutrino parameters that these can be regarded as sharp distinctive predictions. Let us briefly describe these constraints.

5.1.1. IO is excluded

Even though by imposing $SO(10)$ inspired conditions one still finds some marginal allowed regions for IO [33], when the strong thermal condition is further imposed, no solution is found and for this reason we do not show any result for IO in the paper.

5.1.2. Neutrino masses

The solutions are found for quite a restricted range of values for the lightest neutrino mass given by $m_1 \simeq 15$–25 meV ($m_1 \simeq 10$–30 meV) for $N^{\rm p,i}_{B-L} = 10^{-1}$ ($N^{\rm p,i}_{B-L} = 10^{-2}$). This range translates into corresponding ranges for m_2, m_3 and $\sum_i m_i$ given in Table 1. The found solution corresponds to NO *semi-hierarchical neutrinos*, with the heaviest neutrino about three times heavier than the two quasi-degenerate lightest ones.

[9] More precisely we have imposed that a relic value of the pre-existing asymmetry contributes to the final asymmetry less than 10%. Notice that we had to select.

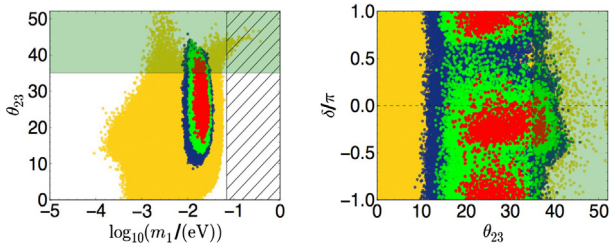

Fig. 4. Result of the scatter plot in the plane θ_{23} vs. m_1 (left) and δ vs. τ_{23} (right) as in Fig. 1 but with θ_{23} let free to variate in a range $0 \leqslant \theta_{23} \leqslant 50°$.

Table 1
Values of the neutrino masses (in meV) as predicted by strong thermal $SO(10)$-inspired leptogenesis.

$N^{\mathrm{p,i}}_{B-L}$	m_1	m_2	m_3	$\sum_i m_i$	m_{ee}
10^{-1}	15–25	17–26	51–55	84–106	12–22
10^{-2}	10–30	13–31	50–57	73–118	9–27

5.1.3. Reactor mixing angle

As one can see from the upper central panel, the bulk of the solutions nicely fall within the range now measured by reactor experiments (cf. Eq. (2)) indicated in the plot. For $N^{\mathrm{p,i}}_{B-L} = 10^{-1}(10^{-2})$ there is a lower bound $\theta_{13} \gtrsim 2°(0.5°)$.

5.1.4. Atmospheric mixing angle

The strong thermal condition cannot be realised for too large values of the atmospheric mixing angle (upper right panel and central left panel). This results into an interesting upper bound $\theta_{23} \lesssim 41°(43°)$ for $N^{\mathrm{p,i}}_{B-L} = 10^{-1}(10^{-2})$ that provides quite a significant test of the solution, since the allowed range is consistent only with current lowest experimentally allowed values.

Since the allowed region clearly extends to values of θ_{23}, lower than those currently allowed by global analyses, we also determined the lower bound of this region repeating the scan for a wider θ_{23} range compared to Eq. (35), extending to values as low as zero. The result is shown in Fig. 4 and one can see that θ_{23} can be as low as $\simeq 16°(13°)$ for $N^{\mathrm{p,i}}_{B-L} = 10^{-1}(10^{-2})$.[10]

5.1.5. Majorana phases

The allowed regions for the Majorana phases close up around special values. There are two different kinds of regions: four centred around $(\sigma, \rho) = (0.8 + n, 1.25 + n)\pi$, with $n = 0, 1$ and four centred around $(\sigma, \rho) = (0.7 + n, 0.75 + n)\pi$, with $n = 0, 1$. These regions are not perfectly coincident to those obtained without imposing the strong thermal condition for $\alpha_2 = 4$ [33]. This shows that they shrink not just around the values that maximise the asymmetry irrespectively of the strong thermal condition, but that the strong thermal condition influences the values of the Majorana phases.

[10] Notice that in this figure the upper bound is more restrictive than in Fig. 1: $\theta_{23} \lesssim 40°$. This is simply due to the fact that in this figure we did not generate enough points to saturate the bounds. We comment on this aspect of the constraints at the end of Section 6.

Table 2
Summary of the set of conditions on low energy neutrino data from $SO(10)$-inspired strong thermal leptogenesis imposing the wash-out of a pre-existing asymmetry as large as 10^{-1} and 10^{-2}.

$N^{\rm p,i}_{B-L}$	10^{-1}	10^{-2}
θ_{13}	$\gtrsim 2^\circ$	$\gtrsim 0.5^\circ$
θ_{23}	$\lesssim 41^\circ$	$\lesssim 43^\circ$
Ordering	Normal	Normal
δ	$(-\pi/2)$–$(\pi/5)$	$\notin [0.4\pi, 0.7\pi]$
	$\simeq \pi$ (marginal, only for $\theta_{23} \lesssim 36^\circ$)	
m_1	15–25 meV	10–30 meV
m_{ee}	$\simeq 0.8 m_1 \simeq$ 12–20 meV	8–24 meV

5.1.6. $0\nu\beta\beta$ *effective neutrino mass* m_{ee}

From the calculation of the effective $0\nu\beta\beta$ effective neutrino mass, $m_{ee} = |\sum_i m_i U_{ei}^2|$, we find that this is quite sharply related to the lightest neutrino mass, and just slightly lower, approximately $m_{ee} \simeq 0.8 m_1$. This is clearly an effect of the quite restricted range of allowed values for the Majorana phases. We will be back on this point when we will discuss the experimental implications of the solution. The allowed range of values for m_{ee} is indicated in the last column of Table 1.

5.1.7. *Dirac phase and* CP *violation*

Very interestingly, having now imposed the strong thermal condition, the Dirac phase and $J_{\rm CP}$ show a preference for negative values. In particular, within the measured range for θ_{13} (cf. Eq. (2)), the Dirac phase falls dominantly in the range $-0.5 \lesssim \delta/\pi \lesssim 0.2$ for $N^{\rm p,i}_{B-L} = 10^{-1}$. Correspondingly one has that the Jarlskog invariant falls in the range $-0.04 \lesssim J_{\rm CP} \lesssim 0.02$. There is also a sub-dominant region for $|\delta|/\pi \simeq 0.9$–1. However, this marginal region exists only for $\theta_{23} \lesssim 36^\circ$. This can be seen from a plot δ vs. θ_{23} that we are not showing in Fig. 1 but we are showing it in Fig. 4 (right panel) for an extended range of θ_{23} but, as discussed, for a reduced data set. As one can see, values $\delta \simeq \pi$ are found even only for $\theta_{23} \lesssim 35^\circ$. This is interesting interplay between δ and θ_{23}.

5.1.8. *Summary*

We summarise in Table 2 the main features of the solution sorted according to a possible chronological order of their experimental test. The first line is the lower bound on the reactor neutrino mixing angle that has been already successfully tested.[11]

5.2. *Constraints on flavour decay parameters*

The natural parameter of leptogenesis are the nine flavoured asymmetries $\varepsilon_{i\alpha}$ and the nine flavour decay parameters $K_{i\alpha}$. As we have seen these can be re-expressed in terms of the nine parameters in the low energy neutrino matrix and of the nine theoretical parameters, six to describe the V_L and the three eigenvalues of the neutrino Dirac mass matrix. In order to have a

[11] Preliminary results on the lower bound on θ_{13} and on the upper bound on θ_{23} were presented in [50].

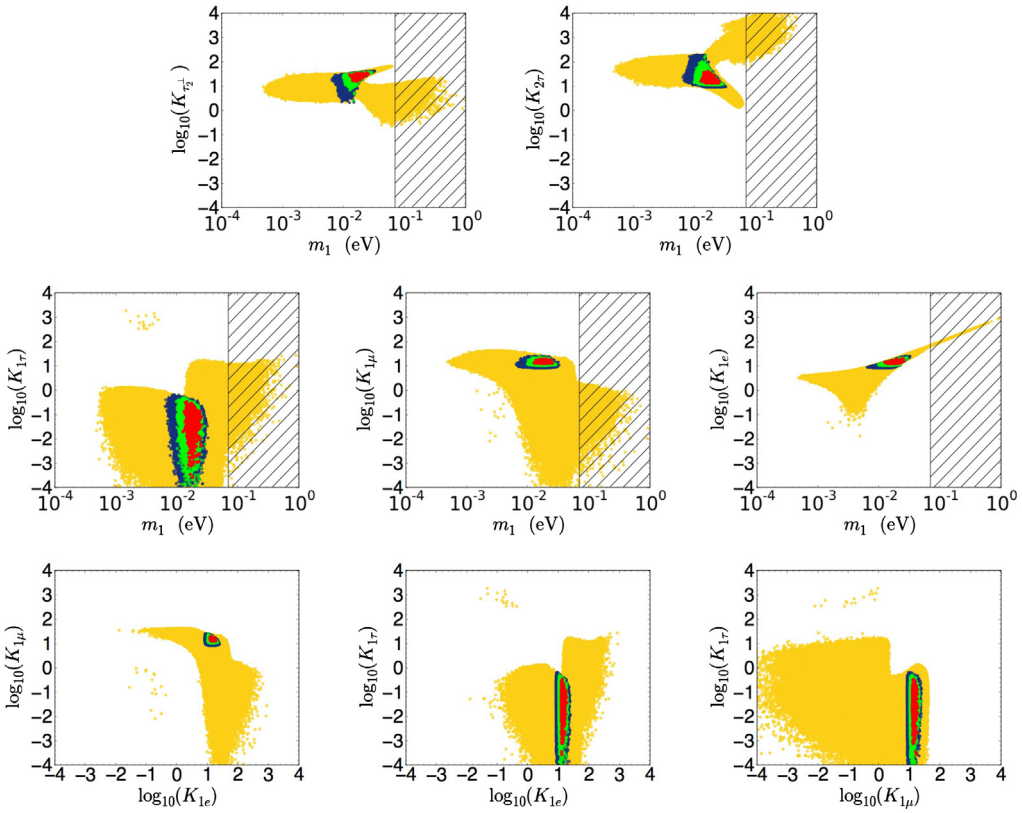

Fig. 5. Results of the scatter plots for the decay flavoured parameters plotted versus either m_1 (first two rows) or versus themselves (only for the $K_{1\alpha}$'s).

useful insight on the constraints on the low energy neutrino parameters discussed in the previous subsection, we show in Fig. 5 plots of the flavour decay parameters $K_{1\alpha}$. In this way we can see what are the values of the relevant flavour decay parameters that realise the strong thermal condition. These plots confirm that the solution we have found realises the conditions (48).

Let us discuss them in more detail. In the lower panels of Fig. 5 we have plotted the flavour decay parameters $K_{1\alpha}$ versus each other. These panels clearly confirm that the conditions Eq. (48) are indeed fulfilled. It is in particular interesting to notice how the two conditions $K_{1e}, K_{1\mu} \gg 1$ are satisfied only for the particular subset of the region realising $SO(10)$-inspired leptogenesis.

Looking at the panels where the $K_{1\alpha}$'s are plotted versus m_1, one can see that the condition $K_{1e} \gg 1$ can only be satisfied for $m_1 \gg 10^{-3}$ eV, while the condition $K_{1\mu} \gg 1$ can only be satisfied for $m_1 \lesssim 0.1$ eV. In addition the plot $K_{2\tau}$ vs. m_1, in the bottom right panel, shows that $K_{2\tau} \gg 1$ implies $m_1 \lesssim 30$ meV, further restricting the upper bound on m_1. In this respect, notice that in that panel one has not to consider the region extending at $K_{2\tau} \gtrsim 100$ and m_1 larger than 0.1 eV, since this corresponds to the muon type solutions. Therefore, the quite narrow range of values of m_1 realising successful strong $SO(10)$ inspired leptogenesis is a consequence of the dependence of the relevant $K_{i\alpha}$ on m_1 in combination with the strong thermal conditions.

5.3. Link between the sign of the asymmetry and the sign of CP violation

The results for the Dirac phase δ and for $J_{\rm CP}$, showing an asymmetry between positive and negative sign values with negative values clearly favoured, are quite interesting and motivate an understanding of their origin. The only physical quantity that can favour one sign compared to the other is the same positive sign of the observed matter–antimatter asymmetry. Therefore, we performed a simple check, working out again the constraints on δ and on $J_{\rm CP}$ but this time imposing $\eta_B^{\rm lep} = -\eta_B^{\rm CMB}$ (in practice we imposed $\eta_B^{\rm lep} < -5.9 \times 10^{-10}$). The results are shown in the right panels of Fig. 5 and compared with those of Fig. 1 displayed again in the left panels. One can see that despite the much lower amount of points in the data set, they clearly show that now the favoured ranges of δ and J switch to positive values. Therefore, we can conclude that the solution favours values of δ and $J_{\rm CP}$ with opposite sign compared to the values of the matter–antimatter asymmetry.

5.4. Are low energy neutrino data pointing in the right direction?

We repeated the same test as in the case of $SO(10)$-inspired leptogenesis finding the constraints on low energy neutrino parameters without any restriction from low energy neutrino experiments. The results are shown in the same Fig. 6. The allowed regions (red, green and blue points) are again subsets of those obtained without imposing the strong thermal condition (yellow points). This time the allowed regions represent a much smaller fraction compared to the whole parameter space and, therefore, an agreement with experimental data would be much more statistically significant.

Let us briefly discuss these results focusing first on the upper panels showing the allowed regions for the mixing angles versus m_1. First of all one can again notice that for negative values of the mixing angles one obtains mirrored regions. Let us then concentrate on positive values of the mixing angles.

One can see that there are two well distinguished allowed regions: a much larger one for 10^{-4} eV $\lesssim m_1 \lesssim 10^{-2}$ eV and a smaller one for 10^{-2} eV $\lesssim m_1 \lesssim 3 \times 10^{-2}$ eV (for $N_{B-L}^{\rm p,i} = 10^{-1}$).

Both regions are compatible with the measured value of the solar mixing angle but whilst the first one, at small m_1, would require unacceptably large values of θ_{23} and θ_{13}, the second one, for large m_1, is perfectly compatible with the measured value of θ_{13} but only with the lowest experimentally allowed range of values of θ_{23}, i.e. for $\theta_{23} \lesssim 41^\circ$.

It is interesting that, just within the three mixing angles parameter space, the fraction occupied by the allowed regions is lower than $\sim 10\%$. It should be also added that IO is excluded even in this case. If one also takes into account the allowed values for m_1, we can say that the chance to hit randomly both the allowed regions, for a logarithmic scan of m_1 between 10^{-5} and 0.1 eV, can be quantified to be about 1%. If one considers that the Majorana phases further restrict the values of m_{ee} compared to the general case (see in the bottom left panel in Fig. 1), one arrives to a probability lower than 0.2%. Finally, taking into account the half chances for the mass ordering, one arrives to the conclusion that the solution occupies roughly a portion that represents roughly 0.1% of the total accessible volume in parameter space. This gives an approximated estimation of the statistical significance that a positive test of the solution would have, i.e. it gives an estimation of the probability that the allowed region corresponding to the solution can be centred by the experimental data just accidentally.

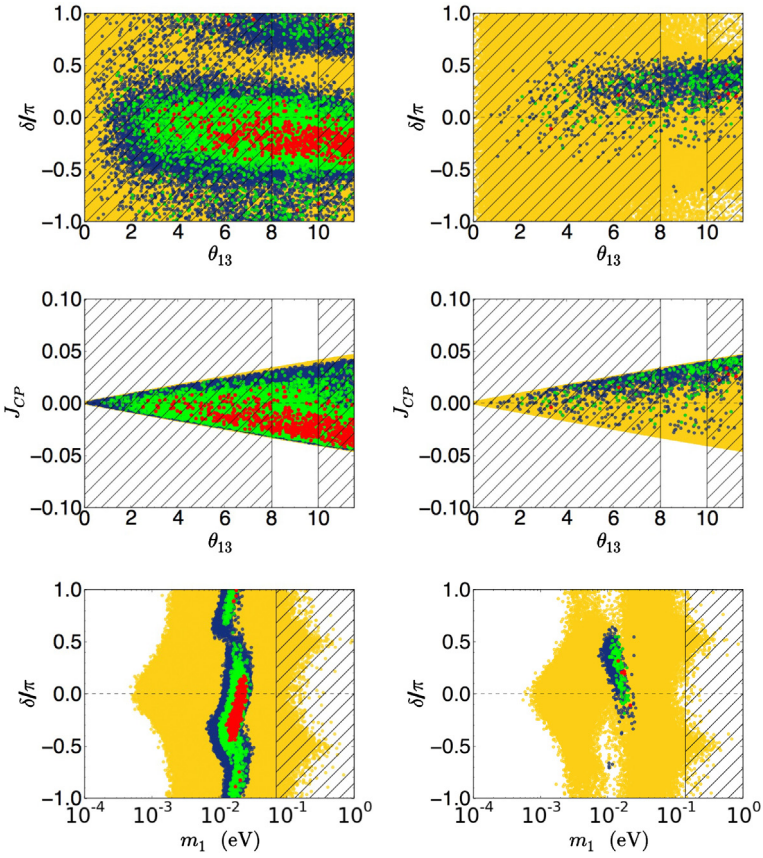

Fig. 6. Results showing how CP violation in neutrino mixing in this scenario is linked to the sign of the matter–antimatter asymmetry. The left panels are obtained imposing $\eta_B^{\rm lep} = \eta_B^{\rm CMB}$, the right panels imposing $\eta_B^{\rm lep} = -\eta_B^{\rm CMB}$.

However, this value of the 'success rate' is dominated by the large excluded region. For the found solution at $m_1 \simeq 20$ meV the success rate would be much smaller, $\sim 10^{-7}$. Imposing the current experimental ranges for the mixing angles (cf. Eqs. (33), (34) and (35)) this rate does not increase simply because, despite the fact that θ_{12} and θ_{13} fall in the allowed regions, the range for θ_{23} Eq. (35) is only marginally compatible. However, if future experimental data will find values $\theta_{23} \lesssim 39°$, the success rate will interestingly increase by an order-of-magnitude. In this case one could say that indeed low energy neutrino data start to show some convergence around the solution. From this point of view a more precise experimental determination of the atmospheric mixing angle represents, in short terms, a crucial test of the solution.

5.5. *Testing the solution*

A very attractive feature of the solution is that the constraints on neutrino parameters that we have just discussed, summarised in Table 2, can be fully tested. In the case of mixing parameters, even by low energy neutrino experiments that are either already taking data or scheduled. In this respect the large value found for θ_{13}, is not only in agreement with the solution, but it is also

a key ingredient that will make possible to determine the atmospheric mixing angle octant, the neutrino mass ordering and (of course) the Dirac phase during next years.

The atmospheric mixing angle is already now favoured to be non-maximal, as discussed in Section 2. It is also encouraging that in [17] the best fit value is found to be $\theta_{23} \simeq 38°$, quite well inside the allowed region (cf. Fig. 4). By combining T2K and NOνA data, such low values will be either determined within a $\sim 3\sigma$ C.L. range of 2°, excluding the second octant, or otherwise be excluded at $\sim 3\sigma$ [51,52]. At the same time the fact that the solution favours the 'experimentally favourable combination' of NO and negative values of $\delta \sim -40°$, makes also possible a $\sim 3\sigma$ determination of the ordering and of the sign of δ by a combination of T2K and NOνA results [51].[12]

Cosmological observations are potentially able to determine a lightest neutrino mass in the range $m_1 = 15$–25 meV, corresponding to $\sum_i m_i \sim 84$–106 meV, improving the current upper bound Eq. (8). In this respect it is interesting that a combination of the Planck results on Sunayev–Zeldovich cluster counts with Planck CMB results and BAO hints at non-vanishing neutrino masses $\sum_i m_i = (0.22 \pm 0.09)$ eV [55].

Notice that values of $\sum_i m_i \sim 0.1$ eV also correspond to inverted hierarchy (i.e. IO for $m_1 \to 0$). From this point of view it is important that the mass ordering can be independently determined with neutrino oscillation experiments, able to disentangle our semi-hierarchical NO solution from an inverted hierarchical solution.

The allowed range for the $0\nu\beta$ decay effective neutrino mass (cf. Table 2) is certainly the most challenging constraint to be tested. In the bottom right panel of Fig. 1 we have also overimposed the general allowed regions in the plane m_{ee} vs. m_1 from current experiments, both for NO and for IO. As one can see, the allowed region corresponding to the solution falls into a range of m_{ee} that is also corresponding to the values expected for inverted hierarchy. These values are not accessible to current ongoing experiments, nor even to planned experiments such as SUPERNEMO, NEXT, Lucifer, MJD that will at most able to exclude values of m_{ee} above 50 meV (for a recent discussion see [56]). However, there is a great international effort for the study of new experiments able to test values in the range 10–20 meV, since these would exclude inverted hierarchy. Again, it is then important that the mass ordering can independently be determined by neutrino oscillation experiments able to distinguish our NO semi-hierarchical solution from inverted hierarchy.

If both m_1 and m_{ee} will be measured with sufficient precision, a comparison will provide an additional test of our solution that predicts $m_{ee} \simeq 0.8 m_1$, due to the particular values of the Majorana phases.[13] In the bottom right panel of Fig. 1, the region between the black lines is the allowed region from low energy neutrino experiments (no leptogenesis) for NO (lower region) and IO (higher region). For NO the ratio m_{ee}/m_1 can, in general, be in the range $m_{ee}/m_1 \simeq 0.3$–1 (corresponding analytically to $\cos 2\theta_{12} \cos^2\theta_{13} - \sin^2\theta_{13} \leqslant m_{ee}/m_1 \leqslant 1$ [57]). Therefore, a result $m_{ee} \simeq 0.8 m_1 \simeq 15$ meV, would further very strongly support the solution. Notice that a determination of both m_1 and m_{ee} would still not be able to fully determine the two Majorana phases. This would provide ideally an even stronger test of the solution making quite precise predictions on both. However, even if we still miss a way to fully determine the Majorana phases, in case of a multiple agreement of all low energy neutrino experiments with the presented con-

[12] A higher statistically significant determination of the ordering can be obtained with PINGU. This would be between 3σ and 10σ after 5 years of operation depending on the reconstruction accuracies [53]. A combination with Daya Bay II would contribute to further improve the statistical significance [54].

[13] This is easy to see analytically replacing $(\sigma, \rho) \simeq (0.8, 1.25)\pi$ in the expression for m_{ee}.

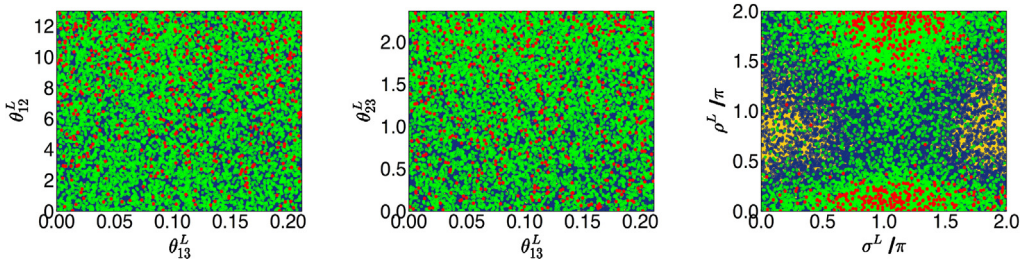

Fig. 7. Results of the same scatter plots as in Fig. 1 for the six parameters in the unitary matrix V_L.

straints, the probability that this is just accidental would be really low (as discussed $\sim 0.1\%$ if one considers both regions together, or even just $\sim 10^{-7}$ if one only considers the discussed solution compatible with current neutrino oscillation data), quite an interesting feature of the solution prospectively.

6. An exploded view of the solution

In this section we discuss some important aspects of the solution.

6.1. Constraints on the parameters in the RH neutrino mixing matrix V_L

We have so far focused on the constraints on the low energy neutrino parameters that can be tested in experiments. However, the solution is also determined by the 6 parameters in the matrix V_L. Indeed the first of the working assumption defining $SO(10)$-inspired models, $I \leqslant V_L \leqslant V_{\rm CKM}$ does not completely fix V_L but allows some variation within a restricted range. In Fig. 7 we show the constraints on the six parameters in the V_L. As one can see from the central panel, the points distribute quite uniformly for θ^L_{23} and θ^L_{13}, indeed the most restricted by the $SO(10)$-inspired condition, while there is a slight preference for high values of θ^L_{12}, maybe an indication for a slight preference of $V_L = V_{\rm CKM}$ compared to $V_L = I$, though solutions for $V_L = I$ are anyway possible.

The points also seem to distribute uniformly in δ_L that, therefore, is not constrained even when the strong thermal condition is added. On the other hand, as it can be seen in the right panel of Fig. 7, the solution favours values of the Majorana-like phases in a region around $(\sigma^L, \rho^L) \simeq (\pi, 0)$.

6.2. A benchmark point

In this subsection we show in Fig. 8 the same plots shown in Fig. 2 in the case of a benchmark point in the space of parameters that does respect the strong thermal leptogenesis. This has been simply chosen as a point that is located in a central position within the 'red' allowed regions ($N^{\rm p,i}_{B-L} = 0.1$).

The results are quite interesting because they show directly how, for $m_1 \simeq 20$ meV and $\theta_{23} \lesssim 41^\circ$, the $K_{i\alpha}$ are indeed able to fulfil all the conditions (48). This benchmark point shows how the strong thermal $SO(10)$-inspired solution is a proper combination of the type τ_A and τ_B solutions discussed in Section 3.2.1 and shown in Fig. 2 for a specific set of values of the parameters. As for the type τ_A solution, there is a sharp dip for $K_{1\tau}$ around a particular value of m_1 such that

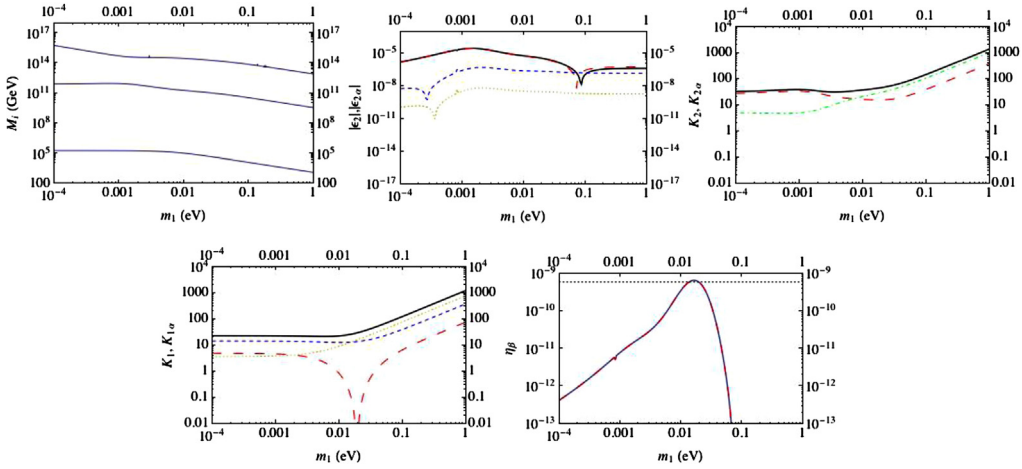

Fig. 8. Plots of the relevant quantities (same set of $(\alpha_1, \alpha_2, \alpha_3)$ values, line and colour conventions as in Fig. 2) for a particular choice of the values of the parameters able to realise successful strong $SO(10)$-inspired leptogenesis for $N^{\rm p,i}_{B-L} = 0.1$. The set of values of the parameters is given by: $\theta_{13} = 9°$, $\theta_{12} = 34°$, $\theta_{23} = 38°$, $\delta = -0.17\pi$, $\rho = 0.20\pi$, $\sigma = 0.87\pi$, $\theta^L_{13} = 0.032°$, $\theta^L_{12} = 6.3°$, $\theta^L_{23} = 2.2°$, $\delta_L = 2.35$, $\rho_L = 0.33$, $\sigma_L = 3.76$.

$K_{1\tau} \lesssim 1$ and in coincidence $K_{1\mu} \gg 1$. However, while for the type τ_A solution one could not respect the condition $K_{1e} \gg 1$ at the dip, now one can see that this is realised as in type τ_B, so that now one has simultaneously $K_{1e} \gg 1$ and $K_{1\mu} \gg 1$. Another important hybrid feature is that now, as for type τ_B, one has $K_{2\tau} \sim 10$ instead of $K_{2\tau} \sim 1000$ as for the type τ_A. This minimises the wash-out of the asymmetry produced by N_2 decays still allowing a wash-out of the pre-existing tauon asymmetry and makes possible to fulfil jointly successful leptogenesis and strong thermal condition.

These are the main features of the solution that can be realised, in particular, only if $m_1 \simeq 20$ meV and $\theta_{23} \lesssim 41°$. Notice that a value $N^{\rm p,i}_{B-L} = \mathcal{O}(0.1)$ represents basically the maximum value of the pre-existing asymmetry that can be washed-out respecting simultaneously the successful leptogenesis bound. The main reason is that $K_{2\tau}$ has to be necessarily much larger than 1 and this necessarily introduces a wash-out at the production. For values $N^{\rm p,i}_{B-L} \gg 0.1$ the value of $K_{2\tau}$ for the wash-out of the pre-existing asymmetry becomes so large that the asymmetry produced by N_2 decays is too strongly washed-out to reproduce the observed asymmetry.

6.3. Stability of the solution

The solution has been determined fixing some parameters and it is then important to discuss whether a variation of these parameters can significantly change the constraints. We have already shown and discussed the dependence on the initial value of the pre-existing asymmetry $N^{\rm p,i}_{B-L}$.

The plots in Fig. 1 have been obtained for $(\alpha_1, \alpha_2, \alpha_3) = (1, 5, 1)$. We verified that indeed there is no dependence of the constraints on α_1 and α_3 as discussed. A value $\alpha_2 = 5$ should be considered close to the maximum within $SO(10)$-inspired models. We have also determined which would be the minimum value of α_2 for the existence of a solution satisfying the strong thermal condition, finding $\alpha_2 \simeq 4$ for $N^{\rm p,i}_{B-L} = 0.1$.

We have checked the sensitivity of the solution to the maximum values of the angles θ_{ij}^L in V_L allowed by the $SO(10)$-inspired conditions. We have tripled the values of θ_{13}^L and θ_{23}^L finding that the only constraint that changes significantly is the upper bound on θ_{23} that is relaxed to $\theta_{23} \lesssim 43^\circ$ for $N_{B-L}^{\rm p,i} = 0.1$. We did not try to modify the Cabibbo-like angle θ_{12}^L since this is already significantly large.

The solution corresponds to a RH neutrino mass spectrum that is genuinely hierarchical since $M_2 \simeq 3 \times 10^{11}$ GeV while $M_3 \simeq \alpha_3^2 10^{14}$ GeV $> 10^{12}$ GeV for $\alpha_3 \gtrsim 0.1$. For example, we have relaxed the condition $M_3/M_2 > 10$ imposed in the results of Fig. 1, redetermining separately the constraints for $10 \geqslant M_3/M_2 \geqslant 2$ finding no new solutions for successful strong thermal leptogenesis.[14] We have found a new different marginal solution only at $m_1 \simeq 0.3$ eV, incompatible with the cosmological bounds. This means that our analysis does not exclude the existence of solutions with quasi-degenerate RH neutrino masses. However, it should be stressed that the strong thermal condition that we have imposed on the relic value of the pre-existing asymmetry (cf. Eq. (47)) is valid only in the hierarchical case. An analysis of the wash-out of a pre-existing asymmetry for quasi-degenerate RH neutrino masses is still missing. In any case it is important to notice that these possible new solutions would in case correspond to different constraints on the low energy neutrino parameters and would be, therefore, experimentally distinguishable from our solution.

6.4. Theoretical uncertainties

Let us now briefly comment on the approximations that we made in the calculation of the asymmetry and on the kind of corrections one could expect removing them.

We are not solving density matrix equations. When we do not impose the strong thermal condition (the yellow points), these can be important when M_2 falls around 10^{12} GeV. For M_2 above 10^{12} GeV we have calculated the asymmetry at the production in the unflavoured case (cf. Eq. (31)). Around $M_2 \simeq 10^{12}$ GeV there is, therefore, a discontinuity. However, since flavour effects, for $M_2 < 10^{12}$ GeV, tend to enhance the asymmetry reducing the wash-out, most of the solutions lie below 10^{12} GeV. When we impose the strong thermal condition for non-vanishing $N_{B-L}^{\rm p,i}$, we have simply excluded points for $M_2 \gtrsim 10^{12}$ GeV, since the strong thermal condition can be satisfied only if the N_2 wash-out occurs in the two-flavour regime. This is the reason why the allowed regions satisfying the strong thermal conditions sharply cut above $M_2 = 10^{12}$ GeV. A calculation from a solution of the density matrix equation would then just simply smoothly describe the transition but this would not significantly affect the results found on the constraints on the low energy neutrino parameters since the bulk of points are found for $M_2 \simeq 3 \times 10^{11}$ GeV.

We are neglecting phantom terms [42]. These can affect the $SO(10)$-inspired solutions (the yellow points) but not certainly the strong thermal $SO(10)$-inspired solution since phantom terms can only be present in the electron and muon asymmetries that are fully washed-out, while the final asymmetry is strictly tauon dominated.

We are neglecting the running of neutrino parameters from the high energy scales to low energies. However, since our solution is semi-hierarchical and NO, the running is negligible for all practical purposes [43]. For the atmospheric mixing angle, the only parameter for which it could be potentially relevant to calculate the running, since we have found compatibility only

[14] We adopted the hierarchical limit for the calculation of the asymmetry. In this limit the wash-out of N_3 on the asymmetry produced by the N_2 is neglected. This would start to produce some effect only for $(M_3 - M_2)/M_2 \lesssim 1$ [58].

with the lowest allowed experimental values, the running is at most about 0.01° from $M_2 \sim 10^{11}$ GeV to low energies, a variation that clearly is completely negligible for any practical purpose.

A potential important correction is flavour coupling [42]. This can have two effects: it can alter the asymmetry at the production, usually this goes in the direction of increasing the asymmetry, and it could make the conditions for strong thermal leptogenesis tighter. The two effects would tend even to cancel with each other. Notice, however, that the flavour coupling would disappear in the limit $K_{1\tau}/(K_{1e}+K_{1\mu}) \to 0$, since this would correspond to a case where the tauon flavour decouples. However, this is exactly the case realised in the solution and, therefore, again, we do not expect great effects from flavour coupling at the lightest RH neutrino wash-out. The only effect might be a small enhancement of the asymmetry at the production that could slightly relax the constraints. The atmospheric neutrino mixing angle upper bound is the most sensitive constraint to corrections and, therefore, this might motivate an account of flavour coupling.

An account of momentum dependence also does not produce significant corrections since this can alter the lightest RH neutrino wash-out only for $K_{1\alpha} \gg 1$ [59], while in our case the production occurs in the tauon flavour and $K_{1\tau} \lesssim 1$.

In conclusion we cannot envisage sources of significant corrections, though an account of flavour coupling might be justified by a precise determination of the upper bound on the atmospheric mixing angle in connections with future experimental results.

6.5. The orthogonal and the RH neutrino mixing matrices

It is also interesting to discuss the form of the RH neutrino mixing matrix U_R and of the orthogonal matrix Ω corresponding to the solution. For the set of values of the parameters corresponding to the benchmark point discussed in Section 6.2, in particular $(\alpha_1, \alpha_2, \alpha_3) = (1, 5, 1)$, and for $m_1 = 20$ meV, the resulting RH neutrino mixing matrix U_R is given by

$$U_R \simeq \begin{pmatrix} e^{-i0.8\pi} & 5\times 10^{-4} e^{i0.6\pi} & 8\times 10^{-6} \\ 5\times 10^{-4} e^{i0.6\pi} & e^{-i\pi} & 2\times 10^{-2} e^{i0.3\pi} \\ 1.5\times 10^{-6} e^{-i0.2\pi} & 2\times 10^{-2} e^{-i0.2\pi} & e^{i0.15\pi} \end{pmatrix}. \tag{49}$$

Contrarily to the final asymmetry and to the $K_{i\alpha}$, the U_R depends not only on α_2 but also on α_1 and α_3 in a way that off-diagonal terms tend to be damped for a higher hierarchy. For example if we choose $(\alpha_1, \alpha_2, \alpha_3) = (5, 5, 5)$, so that M_3/M_2 increases while M_2/M_1 decreases, we obtain

$$U_R \simeq \begin{pmatrix} e^{-i0.8\pi} & 3\times 10^{-3} e^{i0.6\pi} & 8\times 10^{-6} \\ 3\times 10^{-3} e^{i0.6\pi} & e^{-i\pi} & 3\times 10^{-3} e^{i0.3\pi} \\ 1.5\times 10^{-6} e^{-i0.2\pi} & 3\times 10^{-3} e^{-i0.2\pi} & e^{i0.15\pi} \end{pmatrix}, \tag{50}$$

showing that the 23 off-diagonal entries decreased while the 12 increased and the 13 stayed constant. A more drastic enhancement of the, for example, 23 off-diagonal terms is obtained lowering α_3 to $\alpha_3 = 0.05$ obtaining $(\alpha_1 = 1, \alpha_2 = 5)$

$$U_R \simeq \begin{pmatrix} e^{-i0.8\pi} & 5\times 10^{-4} e^{-i0.4\pi} & 1.5\times 10^{-4} e^{-i0.1\pi} \\ 5\times 10^{-4} e^{i0.6\pi} & 0.95 & 0.3 e^{i0.3\pi} \\ 3\times 10^{-5} e^{-i0.2\pi} & 0.3 e^{i0.9\pi} & 0.95 e^{i0.15\pi} \end{pmatrix}. \tag{51}$$

These three examples show how there is a flexibility in the choice of α_1 and α_3 that can potentially be useful in order to minimise the fine tuning to obtain a softly semi-hierarchical light

neutrino mass spectrum ($m_3/m_2 \simeq 3$, $m_2 \simeq m_1$) from highly hierarchical neutrino Yukawa couplings [60].

On the other hand, the orthogonal matrix Ω is very slightly dependent on $(\alpha_1, \alpha_2, \alpha_3)$. This can be calculated from [24]

$$\Omega = D_m^{-\frac{1}{2}} U^\dagger V_L^\dagger D_{m_D} U_R D_M^{-\frac{1}{2}}. \tag{52}$$

For the benchmark choice of parameters one finds

$$\Omega \simeq \begin{pmatrix} 0.8e^{-i0.9\pi} & 0.7e^{i0.1\pi} & 0.4e^{-i0.7\pi} \\ 0.7e^{i0.9\pi} & 0.7e^{-i0.7\pi} & 0.8 \\ 0.4e^{-i0.2\pi} & 0.7 & 0.7e^{i0.1\pi} \end{pmatrix}. \tag{53}$$

The very slight dependence of the orthogonal matrix on α_1 and α_3 is consistent with the independence of the $K_{i\alpha}$ of α_1 and α_3 and, consequently, combined with the independence of $\varepsilon_{2\tau}$ of α_1 and α_3 [33], of the constraints on the low energy neutrino parameters we obtained as well.

This kind of orthogonal matrix (cf. Eq. (53)) shows that there are no fine-tuned cancellations in the see-saw formula. However, each light neutrino mass m_i receives contribution from all three terms $\propto 1/M_j$, not just from one as in the case of an orthogonal matrix close to the identity or to one of the other five forms obtained from the identity permuting rows and columns [22], so-called form dominance models [61].

6.6. Remarks on future developments

We comment on two aspects that will be discussed in detail in future works [62]. First, analytic insight into the results obtained from the scatter plots would be certainly desirable requiring a dedicated analysis.

Second, our analysis does not specify the confidence level of the constraints on the different low energy neutrino parameters. This requires a full determination of the probability distribution functions for the different parameters. This will also be discussed in a future work. Here we just want to notice that these distribution functions are highly non-trivial to determine since even though one starts, as input, from simple Gaussian experimental ranges, the complicated dependence of the asymmetry on the parameters makes in a way that the successful leptogenesis bound and the strong thermal condition produce, as output, quite complicated distributions functions to be determined with a statistical procedure.[15] For example the difference in the upper bounds on θ_{23} in Fig. 1 and in Fig. 4 is an indication of a different C.L., since they are determined with two data sets with a substantial different number of points. Consider the case of an initial pre-existing abundance $N_{B-L}^{\mathrm{p,i}} = 0.1$. In the first case a number of about two thousand red points was obtained to saturate the bound $\theta_{23} \lesssim 41°$, given that the initial ranges for the uniform scan on the low energy neutrino parameters are fixed. The C.L. on this bound corresponds roughly to $\simeq 99.95\%$. In the second case the number of red points is much lower, about three hundreds and the upper bound, $\theta_{23} \lesssim 40°$, does not saturate the maximum value. The C.L. in this case corresponds roughly to 99.7%. This implies that a future experimental result $\theta_{23} \gtrsim 40°$ would strongly disfavour the solution. A precise determination of θ_{23} will be, therefore, a crucial test for the solution.

[15] For some preliminary results see [50].

7. Final discussion

We presented a novel solution to the problem of the initial conditions in leptogenesis within $SO(10)$-inspired models. It is particularly interesting that this yields definite constraints on all low energy neutrino parameters, sharp enough to have, all together, quite a strong predictive power. It is encouraging that the solution requires a non-vanishing value of the reactor mixing angle in agreement with the measured range. This should be considered in addition to the well-known leptogenesis conspiracy for which the solar and atmospheric neutrino mass scales are just about ten times higher than the equilibrium neutrino mass $m_\star \sim 10^{-3}$ eV, in a way that the decay parameters tend to be $K_{i\alpha} = \mathcal{O}(1\text{–}10)$, a key feature for the realisation of the strong thermal condition in the flavoured N_2-dominated scenario. However, the full set of constraints on neutrino parameters from the strong thermal $SO(10)$-inspired solution is still far to be fully tested. As we discussed, it is distinctive enough that it can be regarded as a signature of the solution, hard to be mimicked or to agree just accidentally with the experimental data. It clearly predicts NO neutrino masses, atmospheric mixing angle well in the first octant and it strongly favours a negative Dirac phase, around $\delta \sim -\pi/5$. Indeed these features should all be tested during next years by neutrino oscillation experiments. At the same time the absolute neutrino mass scale predictions, $m_{ee} \simeq 0.8 m_1 \simeq 15$ meV, also provide quite a definite feature that should be tested with cosmological observations and (ultimately with) $00\nu\beta$ decay experiments. It will be exciting to see whether future experimental data will further support the presented solution or rule it out. In any case this provides an example of a motivated falsifiable minimal high energy scale leptogenesis scenario.

Acknowledgements

We wish to thank A. Abada, E. Bertuzzo, S. Blanchet, M. Re Fiorentin, S. King, S.F. King, S. Huber, S. Lavignac, A. Mirizzi, M. Schmidt and T. Yanagida for useful comments and discussions. We acknowledge financial support from the NExT/SEPnet Institute. P.D.B. also acknowledges financial support from the STFC Rolling Grant ST/G000557/1 and from the EU FP7 ITN INVISIBLES (Marie Curie Actions, PITN-GA-2011-289442). L.M. also acknowledges financial support from the European Social Fund (grant MJD387).

References

[1] M. Fukugita, T. Yanagida, Phys. Lett. B 174 (1986) 45.
[2] For recent reviews on leptogenesis see S. Blanchet, P. Di Bari, New J. Phys. 14 (2012) 125012;
T. Hambye, New J. Phys. 14 (2012) 125014.
[3] P. Minkowski, Phys. Lett. B 67 (1977) 421;
M. Gell-Mann, P. Ramond, R. Slansky, in: P. Van Nieuwenhuizen, D. Freedman (Eds.), Proceedings of the Supergravity Stony Brook Workshop, New York, 1979;
T. Yanagida, in: A. Sawada, A. Sugamoto (Eds.), Proceedings of the Workshop on Unified Theories and Baryon Number in the Universe, Tsukuba, Japan, 1979;
R.N. Mohapatra, G. Senjanovic, Phys. Rev. Lett. 44 (1980) 912.
[4] P.A.R. Ade, et al., Planck Collaboration, arXiv:1303.5076 [astro-ph.CO].
[5] S. Blanchet, P. Di Bari, Nucl. Phys. B 807 (2009) 155.
[6] W. Buchmuller, P. Di Bari, M. Plumacher, Phys. Lett. B 547 (2002) 128.
[7] W. Buchmuller, P. Di Bari, M. Plumacher, Ann. Phys. 315 (2005) 305–351.
[8] W. Buchmuller, P. Di Bari, M. Plumacher, Nucl. Phys. B 665 (2003) 445.
[9] A. Abada, S. Davidson, F.-X. Josse-Michaux, M. Losada, A. Riotto, J. Cosmol. Astropart. Phys. 0604 (2006) 004;
E. Nardi, Y. Nir, E. Roulet, J. Racker, J. High Energy Phys. 0601 (2006) 164.
[10] S. Davidson, J. Garayoa, F. Palorini, N. Rius, Phys. Rev. Lett. 99 (2007) 161801.

[11] S. Antusch, P. Di Bari, D.A. Jones, S.F. King, Phys. Rev. D 86 (2012) 023516.
[12] E. Bertuzzo, P. Di Bari, L. Marzola, Nucl. Phys. B 849 (2011) 521–548.
[13] S. Blanchet, P. Di Bari, J. Cosmol. Astropart. Phys. 0703 (2007) 018.
[14] S. Pascoli, S.T. Petcov, A. Riotto, Phys. Rev. D 75 (2007) 083511.
[15] A. Anisimov, S. Blanchet, P. Di Bari, J. Cosmol. Astropart. Phys. 0804 (2008) 033.
[16] K. Abe, et al., T2K Collaboration, Phys. Rev. Lett. 107 (2011) 041801;
P. Adamson, et al., MINOS Collaboration, arXiv:1108.0015 [hep-ex];
Y. Abe, et al., DOUBLE-CHOOZ Collaboration, arXiv:1112.6353 [hep-ex];
F.P. An, et al., DAYA-BAY Collaboration, arXiv:1203.1669 [hep-ex];
S.-B. K. f. R. Collaboration, arXiv:1204.0626.
[17] G.L. Fogli, E. Lisi, A. Marrone, D. Montanino, A. Palazzo, A.M. Rotunno, Phys. Rev. D 86 (2012) 013012.
[18] M.C. Gonzalez-Garcia, M. Maltoni, J. Salvado, T. Schwetz, arXiv:1209.3023 [hep-ph].
[19] D.V. Forero, M. Tortola, J.W.F. Valle, Phys. Rev. D 86 (2012) 073012.
[20] S. Uhlig, J. High Energy Phys. 0711 (2007) 066.
[21] S.F. King, Nucl. Phys. B 576 (2000) 85;
P.H. Frampton, S.L. Glashow, T. Yanagida, Phys. Lett. B 548 (2002) 119;
A. Ibarra, G.G. Ross, Phys. Lett. B 591 (2004) 285;
A. Abada, S. Davidson, A. Ibarra, F.-X. Josse-Michaux, M. Losada, A. Riotto, J. High Energy Phys. 0609 (2006) 010.
[22] P. Di Bari, Nucl. Phys. B 727 (2005) 318–354.
[23] O. Vives, Phys. Rev. D 73 (2006) 073006.
[24] P. Di Bari, A. Riotto, Phys. Lett. B 671 (2009) 462.
[25] W. Buchmuller, M. Plumacher, Phys. Lett. B 389 (1996) 73.
[26] E. Nezri, J. Orloff, J. High Energy Phys. 0304 (2003) 020, arXiv:hep-ph/0004227.
[27] F. Buccella, D. Falcone, F. Tramontano, Phys. Lett. B 524 (2002) 241.
[28] G.C. Branco, R. Gonzalez Felipe, F.R. Joaquim, M.N. Rebelo, Nucl. Phys. B 640 (2002) 202.
[29] E.K. Akhmedov, M. Frigerio, A.Y. Smirnov, J. High Energy Phys. 0309 (2003) 021.
[30] S. Davidson, A. Ibarra, Phys. Lett. B 535 (2002) 25;
W. Buchmuller, P. Di Bari, M. Plumacher, Nucl. Phys. B 643 (2002) 367;
W. Buchmuller, P. Di Bari, M. Plumacher, Nucl. Phys. B 793 (2008) 362 (Erratum).
[31] L. Covi, E. Roulet, F. Vissani, Phys. Lett. B 384 (1996) 169.
[32] A. Pilaftsis, T.E.J. Underwood, Nucl. Phys. B 692 (2004) 303.
[33] P. Di Bari, A. Riotto, J. Cosmol. Astropart. Phys. 1104 (2011) 037.
[34] A. Abada, P. Hosteins, F.-X. Josse-Michaux, S. Lavignac, Nucl. Phys. B 809 (2009) 183.
[35] S. Blanchet, P.S.B. Dev, R.N. Mohapatra, Phys. Rev. D 82 (2010) 115025.
[36] R. Nichol, MINOS Collaboration, Nucl. Phys. B, Proc. Suppl. 235–236 (2013) 105.
[37] J.A. Casas, A. Ibarra, Nucl. Phys. B 618 (2001) 171.
[38] F. Buccella, D. Falcone, C.S. Fong, E. Nardi, G. Ricciardi, Phys. Rev. D 86 (2012) 035012.
[39] R. Barbieri, P. Creminelli, A. Strumia, N. Tetradis, Nucl. Phys. B 575 (2000) 61–77.
[40] G.F. Giudice, A. Notari, M. Raidal, A. Riotto, A. Strumia, Nucl. Phys. B 685 (2004) 89.
[41] S. Blanchet, P. Di Bari, D.A. Jones, L. Marzola, J. Cosmol. Astropart. Phys. 1301 (2013) 041.
[42] S. Antusch, P. Di Bari, D.A. Jones, S.F. King, Nucl. Phys. B 856 (2012) 180.
[43] K.S. Babu, C.N. Leung, J.T. Pantaleone, Phys. Lett. B 319 (1993) 191;
S. Antusch, J. Kersten, M. Lindner, M. Ratz, Nucl. Phys. B 674 (2003) 401;
S. Antusch, J. Kersten, M. Lindner, M. Ratz, M.A. Schmidt, J. High Energy Phys. 0503 (2005) 024.
[44] M. Apollonio, et al., CHOOZ Collaboration, Phys. Lett. B 466 (1999) 415.
[45] T. Schwetz, M.A. Tortola, J.W.F. Valle, New J. Phys. 10 (2008) 113011.
[46] E. Andreotti, et al., Astropart. Phys. 34 (2011) 822;
M. Agostini, et al., GERDA Collaboration, arXiv:1307.4720 [nucl-ex].
[47] R. Kallosh, A.D. Linde, D.A. Linde, L. Susskind, Phys. Rev. D 52 (1995) 912, arXiv:hep-th/9502069;
H. Davoudiasl, R. Kitano, G.D. Kribs, H. Murayama, P.J. Steinhardt, Phys. Rev. Lett. 93 (2004) 201301.
[48] I. Affleck, M. Dine, Nucl. Phys. B 249 (1985) 361.
[49] M. Yoshimura, Phys. Rev. Lett. 41 (1978) 281;
M. Yoshimura, Phys. Rev. Lett. 42 (1979) 746 (Erratum);
S. Dimopoulos, L. Susskind, Phys. Rev. D 18 (1978) 4500;
D. Toussaint, S.B. Treiman, F. Wilczek, A. Zee, Phys. Rev. D 19 (1979) 1036;

E.W. Kolb, S. Wolfram, Nucl. Phys. B 172 (1980) 224;
E.W. Kolb, S. Wolfram, Nucl. Phys. B 195 (1982) 542 (Erratum);
E.W. Kolb, A.D. Linde, A. Riotto, Phys. Rev. Lett. 77 (1996) 4290.
[50] Talks by P. Di Bari, L. Marzola at the DESY Theory Workshop 2011, 27–30 September 2011, Hamburg.
[51] P. Huber, M. Lindner, T. Schwetz, W. Winter, J. High Energy Phys. 0911 (2009) 044.
[52] S.K. Agarwalla, S. Prakash, S.U. Sankar, arXiv:1301.2574 [hep-ph].
[53] E.K. Akhmedov, S. Razzaque, A.Y. Smirnov, J. High Energy Phys. 1302 (2013) 082.
[54] M. Blennow, T. Schwetz, arXiv:1306.3988 [hep-ph].
[55] P.A.R. Ade, et al., Planck Collaboration, arXiv:1303.5080 [astro-ph.CO].
[56] B. Schwingenheuer, Ann. Phys. 525 (2013) 269;
O. Cremonesi, Nucl. Phys. B, Proc. Suppl. 237–238 (2013) 7.
[57] W. Rodejohann, Int. J. Mod. Phys. E 20 (2011) 1833.
[58] S. Blanchet, P. Di Bari, J. Cosmol. Astropart. Phys. 0606 (2006) 023.
[59] J. Garayoa, S. Pastor, T. Pinto, N. Rius, O. Vives, J. Cosmol. Astropart. Phys. 0909 (2009) 035.
[60] J.A. Casas, A. Ibarra, F. Jimenez-Alburquerque, J. High Energy Phys. 0704 (2007) 064.
[61] S.F. King, Rep. Prog. Phys. 67 (2004) 107;
M.C. Chen, S.F. King, J. High Energy Phys. 0906 (2009) 072.
[62] In preparation.